JGR Biogeosciences

RESEARCH ARTICLE
10.1029/2022JG007272

Special Section:
The Earth in living color: spectroscopic and thermal imaging of the Earth: NASA's Decadal Survey Surface Biology and Geology Designated Observable

Hyperspectral Mixture Models in the CHIME Mission Implementation for Topsoil Texture Retrieval

Emiliana Valentini[1,2], Andrea Taramelli[2,3], Chiara Marinelli[2], Laura Piedelobo Martin[2,4], Marco Fassari[1], Stefano Troffa[2], Nada Mzid[5], Raffaele Casa[5], and Stefano Pignatti[6]

[1]Institute of Polar Sciences of the National Research Council of Italy (ISP CNR), Roma, Italy, [2]University Institute for Advanced Study of Pavia (IUSS), Pavia, Italy, [3]Institute for Environmental Protection and Research (ISPRA), Roma, Italy, [4]Department of Cartographic and Land Engineering, University of Salamanca, Ávila, Spain, [5]Department of Agriculture Forestry Sciences (DAFNE), University of Tuscia, Viterbo, Italy, [6]Institute of Methodologies for Environmental Analysis of the National Research Council of Italy, Potenza, Italy

Abstract This study is part of the requirements consolidation study for the European Copernicus Hyperspectral Imaging Mission for Environment (CHIME). It explores the value added by existing hyperspectral data of similar characteristics to CHIME, namely AVIRIS-NG and PRecursore IperSpettrale della Missione Applicativa (PRISMA), for detecting topsoil texture properties. The spatial variability is retrieved using the linear spectral mixture analysis, an image-based algorithm that breaks down the hyperspectral data set into fractional abundance of spectral classes within each pixel. The fractional abundance of image-based endmembers is broken into categories to find intervals having a spatial relation with texture components in terms of fine (clay and silt) or coarse (sand) abundance. The fraction maps obtained show similar spatial patterns to the USDA soil texture classification, obtained with a geostatistical approach. Specifically, AVIRIS CHIME-like FAM1 > 0.45 presented an agreement of 86% with clay and/or silt higher than 45% which, according to the United Stated Agriculture Department (USDA) intervals, correspond to loam-clay loam classes. Similar results are obtained with PRISMA with FAM2 0.20–0.35, overlapping 63% of the kriging-based USDA clay-loam class. The fractional abundance categories showing the highest overlap percentages are correlated with the short-wave infrared spectral range, showing average coefficients of 0.7 where wavelengths are over 1,500 nm. From 1700 nm, CHIME-like shows values of 0.8. In conclusion, this exploratory research and results leverage the opportunity of extending the processing chain to a larger number of case studies to better understand the physical relation between the spectral reflectance captured by new spaceborne hyperspectral sensors and the spatial patterns of soil texture classes.

Plain Language Summary In the current context led by the constant availability, almost in near-real time, of remote sensing data with high spatial, spectral and temporal resolutions, the monitoring of soil properties should no longer be solely limited to field data observations. There is a growing need of knowledge for preserving and exploiting soils and the upcoming generation of hyperspectral satellite remote sensing has popped up new opportunities for developing and adapting algorithms that break up the image pixels into several spectral behaviors that correspond to different soil properties. This paper contributes to the application of these image analysis techniques to soil texture classes retrieval considering the United Stated Agriculture Department model. The paper uses the principles of the spectral mixture concept to explore the opportunity of detecting soil textures in two farmland units and provides some highlights on the observational requirements needed to integrate the future satellite missions' architecture within the agriculture and food security application domain.

Key Points:

- Hyperspectral imaging is used to retrieve United Stated Agriculture Department soil texture classification in two farmland units applying linear spectral mixture analysis
- Copernicus Hyperspectral Imaging Mission for Environment-like and PRecursore IperSpettrale della Missione Applicativa-derived fractional abundance intervals are found to spatially overlap the clay-loam class obtained with field data
- Fractional abundances categories having the highest overlap percentage are strongly correlated with the Short-Wave InfraRed > 1,500 nm

Supporting Information:

Supporting Information may be found in the online version of this article.

Correspondence to:

E. Valentini,
emiliana.valentini@cnr.it

Citation:

Valentini, E., Taramelli, A., Marinelli, C., Martin, L. P., Fassari, M., Troffa, S., et al. (2023). Hyperspectral mixture models in the CHIME mission implementation for topsoil texture retrieval. *Journal of Geophysical Research: Biogeosciences*, *128*, e2022JG007272. https://doi.org/10.1029/2022JG007272

Received 11 NOV 2022
Accepted 30 JUN 2023

Author Contributions:

Conceptualization: Emiliana Valentini, Andrea Taramelli

1. Introduction

To define opportunities of investing in the Sentinel-10/CHIME, the hyperspectral satellite candidate mission by the European Space Agency (ESA) (Rast et al., 2019) the knowledge of soil texture variability is a key factor for (a) site-specific farming management, (b) more efficient use of water and fertilizers, and (c) reducing costs and environmental impacts (Castaldi et al., 2016). The estimation and mapping of soil texture, expressed as the relative proportion of clay, sand and silt, is one of the main users' requirements for the Agriculture and Food Security application domain within the European Union (EU) Copernicus Earth Observation (EO) and monitoring program. Furthermore, the majority of the institutional stakeholders involved in the user-driven requirements collection expressed the need for consolidating algorithms and mapping products for both soil texture and soil

Data curation: Emiliana Valentini, Raffaele Casa, Stefano Pignatti
Formal analysis: Emiliana Valentini, Chiara Marinelli, Laura Piedelobo Martin, Marco Fassari, Stefano Troffa, Raffaele Casa, Stefano Pignatti
Funding acquisition: Andrea Taramelli
Investigation: Emiliana Valentini, Chiara Marinelli, Laura Piedelobo Martin, Raffaele Casa, Stefano Pignatti
Methodology: Emiliana Valentini, Laura Piedelobo Martin
Supervision: Emiliana Valentini, Andrea Taramelli, Laura Piedelobo Martin
Validation: Emiliana Valentini
Visualization: Emiliana Valentini, Chiara Marinelli
Writing – original draft: Emiliana Valentini, Chiara Marinelli, Laura Piedelobo Martin, Marco Fassari, Stefano Troffa

organic content (Taramelli et al., 2020) These requirements are related to the monitoring of the impacts and the effects of agricultural and environmental policies (Taramelli et al., 2019), such as the European Common Agricultural Policy (CAP) for 2021–2027. In this framework, the CHIME Requirements Consolidation Study (RCS), funded by ESA jointly with the EU, was specifically tasked on evaluating whether the development of a new Copernicus Sentinel hyperspectral satellite mission could satisfy these users' requirements with specific observational sensor characteristics (Rast et al., 2019).

Soil is essential for life and vital to solving global environmental challenges such as food and water security, climate change adaptation and biodiversity protection (Arrouays et al., 2017).

Precision agriculture is becoming the major opportunity for improving food security through optimal management and sustainable use of arable lands. One of the most relevant soil properties to be considered in precision agriculture is the soil texture since it determines the degree of water penetration and retention, nutrient absorption, susceptibility to erosion, germination and rooting of agricultural crops (Phogat et al., 2015). Soil water content is also influenced by texture and organic carbon contents. It has been demonstrated that low organic matter content enhances the water retention capacity in sandy soils while high organic content determines increases in water retention for all textures even if larger in sandy and silty soils (Rawls et al., 2003). Optimal irrigation management practices require estimation of soil–water retention for many crops since it is essential for optimizing the water use considering soil infiltration, hydraulic conductivity and the available water holding capacity of plants. Sandy-textured soils hold less water and drain relatively faster than clayey-textured soils. In sandy soils, most of the pores drain shortly after a rainfall or irrigation and the capillary conductivity in these soils becomes negligibly small at high soil–water matric potentials compared to clayey soils (Jabro et al., 2009). There is an increasing gradient of water and nutrient holding capacity from coarse to finer texture classes and clayey soils are usually less prone to wind and rain erosion because of the degree of particles aggregation and the higher presence of organic content that supports sealing properties. Given that, the importance of soil texture for resistance to erosive factors is evident, particularly in arid and semi-arid regions, where the soils are predominantly calcareous with low organic matter content and weakly aggregated structures which are more susceptible to water erosion processes (Vaezi et al., 2016).

Globally, soil degradation and erosion are expected not only to have an impact on the vulnerability of soil conditions but also on soil biodiversity, with 6.4% (for soil macrofauna) and 7.6% (for soil fungi) of vulnerable areas coinciding with regions with high soil biodiversity (Guerra et al., 2020). Soil biological communities (i.e., microbial bacteria, fungi and protists together with invertebrates macrofauna), having a key role in a wide range of soil related biogeochemical cycles and organic matter decomposition, are the invisible base of biodiversity and they are constrained by soil organic content and soil abiotic properties, as pH, moisture and texture (Seaton et al., 2020). Soil abiotic properties, such as pH, moisture and texture, directly affect soil biodiversity through their effects on plant communities, which are known to maintain soil biomes by concentrating resources, biomass and litter. Moreover, bacteria, are constrained by soil pH and carbon availability, preferring the biofilms around stable and fine-textured soils (Ding & Eldridge, 2022).

In the agricultural sector, a better understanding of soil properties, including texture, is essential to face ongoing challenges concerning the production of safe, high-quality, affordable, nutritious, and diverse food (UN Sustainable Development Goals 2 and 12) (Bouma et al., 2021). The potential importance of the range of soil particles stimulate the exploration of emerging technologies and new analytical methods in retrieving soil texture, soil organic content and soil moisture.

The use of optical remote sensing and in particular the exploitation of the visible, near-infrared and shortwave infrared (VIS-NIR-SWIR, 400–2,500 nm) spectral region, is very effective for the study of physical and chemical topsoil properties, allowing for reducing the need of extensive sampling campaigns and laboratory analyses (Ben-Dor et al., 2018; Safanelli et al., 2020). VIS-NIR hyperspectral imaging techniques are mostly based on the study of the specific vibrations of chemical bonds between molecules (Mohamed et al., 2018). Within the VIS (400–700 nm) spectral region, the electronic transitions produce wide absorption bands caused by the chromophores that influence the soil color, while in the NIR – SWIR (700–2,500 nm) spectral region, weak shades and combinations of vibrations are generated, due to the stretching and bending of the OH, CH and NH bonds (Viscarra Rossel et al., 2006). Topsoil properties (i.e., soil texture and organic content) are thus difficult to be estimated with broadband multispectral data as the absorption peculiarities cannot be fully resolved due to the coarse spectral resolution in the 1,100–2,400 nm spectral range. NIR-SWIR spectral ranges correspond to the spectral

regions most affected by the topsoil chromophores (Ben-Dor et al., 2009; Castaldi et al., 2016). Bare soils have shown considerable potential for the estimation of topsoil texture and the finer bandwidth offered by hyperspectral in comparison to multispectral data, allows for developing physically based approaches (Casa et al., 2013). The other side of the retrieval is strictly related to the spatial resolution because few studies provide a solid discussion on the issue and it seems that 5–30 m gave similar performance of prediction, for instance for clay (Gomez et al., 2015). In Casa et al. (2020), comparable results were obtained for clay estimation at 20 and 30 m, whereas the retrieval accuracy for sand, silt, and soil organic carbon (SOC) was slightly worse than for clay.

Nowadays the number of satellite hyperspectral missions for environmental monitoring is rapidly increasing. Already orbiting hyperspectral satellites are the Italian PRISMA (PRecursore IperSpettrale della Missione Applicativa), launched in 2019 (Cogliati et al., 2021), and the German EnMAP (Environmental Mapping and Applications Program) launched in 2022 (Bachmann et al., 2021). The panorama of spaceborne hyperspectral imagers, is enriched by operational sensors on the International Space Station (ISS) as the recently launched (2022) NASA's EMIT (Earth Surface Mineral Dust Source Investigation) (Green & Thompson, 2021), DESIS (German Aerospace Center (DLR) Earth Sensing Imaging Spectrometer) launched in 2018 as a precursor instrument for EnMAP (Krutz et al., 2019) and the Japanese HISUI (Hyperspectral Imager Suite), operational on ISS since 2020 (Matsunaga et al., 2022). These monitoring programs will be soon enlarged by the candidate satellite missions HyspIRI (Hyperspectral InfraRed Imager) supported by the US-NASA SBG initiative (Surface Biology and Geology) (Lee et al., 2015) and by CHIME (Copernicus Sentinel 10) supported by the European Union through ESA (Nieke & Rast, 2018).

These hyperspectral imagers cover wavelengths from 400 to 1,000 nm (VNIR) and from 900 to 2,500 nm (SWIR) with high spectral resolutions spanning from 7 to 12 nm. With continuous narrow bands, particularly in the SWIR region, these sensors provide the possibility of enhancing the accuracy of soil texture, moisture and organic content retrieval (Castaldi et al., 2016). Moreover, users' benefit is improved by the diversity of data sources and resolutions. Hyperspectral imagery, with the continuous spectral sampling, coupled with the wider spatial coverage, spatial resolution and short revisit time of multispectral sensors, like Sentinel 2 and Landsat 8–9, represent an unprecedented synergy for topsoil properties retrieval (Guanter et al., 2015).

By side to this availability of spaceborne hyperspectral sensors, there is a parallel increase in the development of methods for the generation and delivery of soil thematic products to the geoscience community (Chabrillat et al., 2019; Mzid et al., 2022). Currently, for soil thematic mapping, most of the existing products are highly dependent on field and laboratory radiometric measurements, making the retrieval algorithms still very locally accurate. In this sense, there is an increasing interest in the potential of global standardized soil spectral libraries databases (e.g., LUCAS—Land Use/Land Cover Area Frame Survey) that could support globally applicable methodologies suitable to process the spectral data into practical soil properties models (Viscarra Rossel et al., 2016).

The aggregate effects of high spectral mixed variance an the spatial composition within each pixel can be modeled by treating the observed reflectance, as a linear mixture of a small set of generic endmembers (EMs) spectra (Sousa et al., 2022). The high spectral dimensionality of hyperspectral data could be associated with an EMs collection representing either the spatial homogeneity or the heterogeneity of bare soil agricultural units and allowing the implementation of linear spectral mixture models within each pixel of the scene (Valentini et al., 2020). Linear Spectral Mixture Analyses (LSMA) is generally limited when the reflectance behavior of the EMs captured by the mixing space are less than in the reality or when the reality is rich of many unknown physical targets (Sousa & Small, 2018). Nevertheless, when the application of the mixture models is constrained to fit a small number of endmembers (EMs), such as the retrieval of sand, silt and clay, the high number of spectral bands enables to capture the spatial dimensionality of the system and a technique like the LSMA provides a stimulating opportunity to support topsoil texture retrieval at an agricultural farmland unit scale.

Within CHIME High Priority Products, the soil textural composition has been consolidated using multivariate modelling like Partial Least Squares Regression (PLSR) and Random Forests (RF) algorithms. Results of these models were based on existing local or regional soil spectral libraries and on field samples for the calibration and the validation of the models. Some good result was obtained for clay estimation, whereas for sand, silt, and soil organic carbon (SOC) the retrieval accuracy was slightly worse (Casa et al., 2020) determining the need for further research in the field of soil texture retrieval. The purpose of testing LSMA is then to open new windows

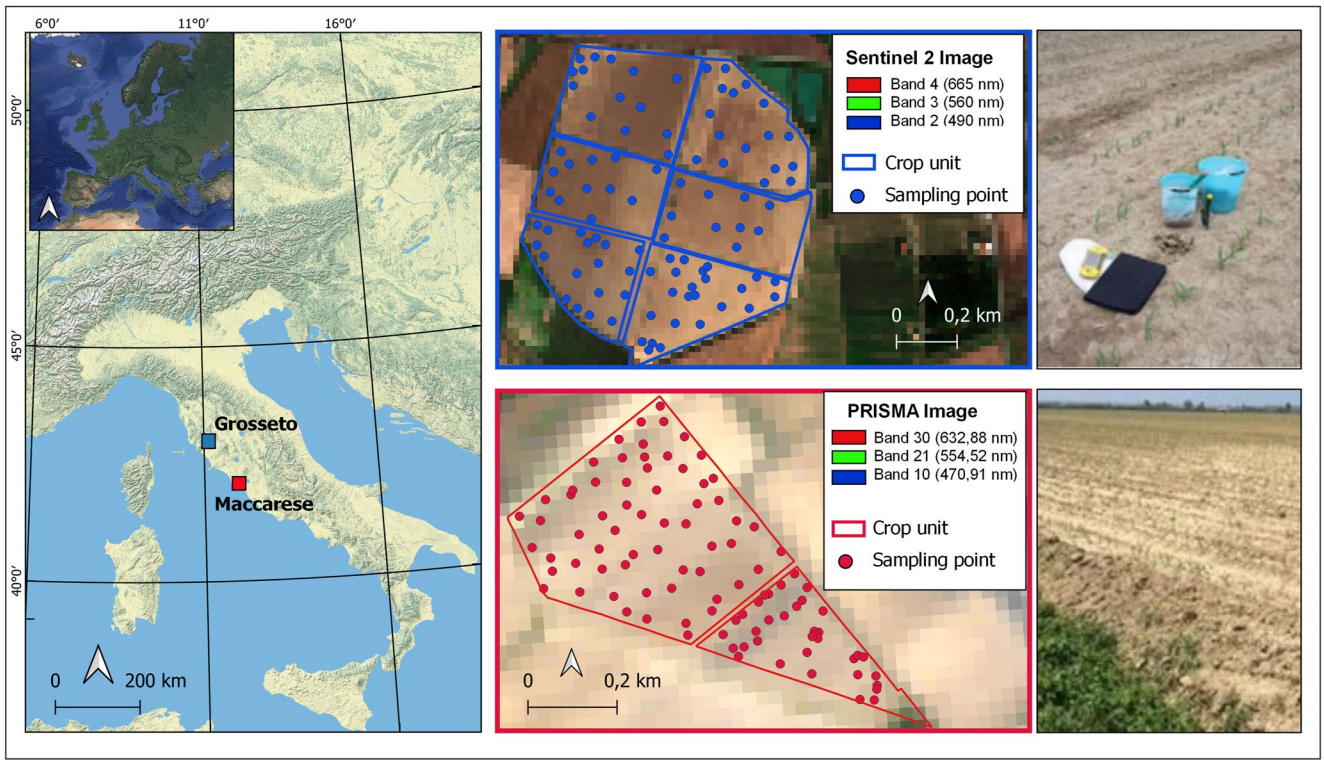

Figure 1. Study areas: with blue box: Braccagni cropland boundaries and field sampling points. The base map is a RGB composite from Sentinel 2 of 14 May 2020; with red box, Maccarese cropland and field sampling points. The base map is a RGB composite from PRISMA of 8 February 2020. On the right the view of the field condition at the time of image acquisition.

on soil texture detection having consequent optimization and improvement of retrieval schemes and fulfilling the objectives of the CHIME mission by tuning different retrieval models including secondary algorithms.

This study explores a novel view in techniques for hyperspectral image analysis to treat the dimensionality problem taking into account both the spectral and spatial properties of the data. The LSMA, is used in its basic geometric formulation and exploits an expert "user-supplied" collection of EMs spectra, without introducing any automatism but using only the image captured variance. In this way the physical dimension of the problem is always interpretable and suitable of understanding the existence of a relation between the spectral fractions and the spatial distribution of textures. This approach is aimed at including in the hyperspectral imaging data processing the spatial dimension of the variability in topsoil texture retrieval. The study explores the opportunities offered by spectral mixture models to fully exploit the VIS-NIR-SWIR spectrum and to estimate fractions of soil texture classes within farmland units of bare soils. Specifically, it compares image based LSMA with the standard USDA soil classification obtained by interpolating and thresholding ground truthing data. The hypothesis is that the spectral dimensionality captured by hyperspectral resolution could be associated more easily to the spatial patterns of soil at class level when working at agricultural units' scale instead of retrieving the composition of each pixel in terms of percentage of sand, silt and clay. The analysis is also oriented towards the detection of specific wavelengths, and synergies among hyperspectral and multispectral sensors including airborne data from AVIRIS NG sensor, resampled according to the spectral configurations of CHIME and Sentinel 2 (CHIME-like, Sentinel 2-like), and original satellite data from PRISMA and Sentinel-2.

2. Materials and Methods

2.1. Study Areas

The topsoil texture retrieval was tested on the bare soil units of two cropland areas in Central Western Italy (Figure 1). The two areas have a Mediterranean climate, characterized by mild and humid winters and hot and dry summers.

The Braccagni test area (Grosseto municipality, Central Italy, 42°49′47.02′′N 11°04′10.27′′E; elev. 2 m a.s.l.) included an irrigated field of 70 ha where maize is cultivated in summer as fodder, following a winter ryegrass crop harvested in early June. During the winter, the minimum night temperatures are commonly below 0°C while in the summer days the maximums are above 30°C (Silvestro et al., 2021). The annual temperature is around 15°C and the average annual rainfall is 640 mm (Candiani et al., 2022). The shape of the field in the study area is circular due to the pivots, self-propelled irrigation systems with mobile towers that ensure uniformity of water distribution through high-frequency watering but with reduced volumes. The soils in Grosseto are classified as Luvisols (Food and Agriculture Organization of the United Nations, 1998) prevailingly falling in the silty clay loam and silt loam texture classes. Soil moisture measurements at the time of image collection are not available. Regarding the soil textures, the field is mainly divided in 2 areas: a clay-rich soil zone in the west portion and a fertile area in the east part.

The Maccarese area (Rome municipality, Central Italy, 41°52′18″ N, 12°14′05″ E; elev. 8 m a.s.l.) is very close to the coast and it is mainly cultivated with maize, durum and winter wheat, fodder crop and broad bean. The climate is characterized by an average annual temperature of 15.5°C and annual rainfall of 734 mm (Xie et al., 2018). The study area underwent reclamation works from marshland to agriculture in the early 1920s, and according to a recent regional soil map the parent materials of the northeastern part of the farmland are alluvial deposits of the Arrone river. The Maccarese soil is classified as Cutanic Luvisol (FAO-ISRIC-ISSS, 2007), with sandy clay loam texture, becoming more clayey toward the north-east of the site. Soil parent materials are flat inshore deposits (Pleistocene). There is no carbonate soil in the site while it is possible to identify shell remains on the dunes (Mzid et al., 2022) because the Maccarese croplands are characterized by the proximity to groups of beach ridges corresponding to eight homogeneous complexes that are part of the delta of the river Tevere.

2.2. Workflow

The methodology used to retrieve textural classes from each image data set starts with the image preprocessing that includes both geometric and radiometric analyses.

Each image data set is then processed using the Linear Spectral Mixture Analyses (LSMA), a soft classification that provides sets of Fractional Abundance Maps (FAMs). After computing FAMs standardization, the processing chain includes the definition of thresholds based upon the frequency distribution of continuous values of these FAMs classifying them into discrete intervals (i.e., low, medium, high values).

Parallel to the image processing, the ground truthing data set is classified following the same intervals used for the FAMs, providing the classes for implementing the validation with the confusion matrix. The validation provided different level of accuracy for each FAM intervals and the best results were selected for masking specific FAMs.

Moreover, the ground truthing data set is interpolated to obtain three raster layers with the spatial distribution of each texture (sand, silt, clay) and used to build a USDA soil classification map. This classification provides the classes to compute zonal statistics with masked-FAMs and, as first output of the analyses, the estimates of the spatial relation between the masked-FAMs and the USDA classes in terms of overlapping soil texture surfaces.

The last step of the processing chain is oriented to the definition of the relevant spectral bands for the soil classes retrieval and it is based on the use of a correlative approach between each masked-FAM and each sensor waveband (Figure 2).

2.2.1. Field Sampling

In both croplands, field campaigns were constrained to completely or quite completely bare soils. All samples were analyzed to determine the clay, silt and sand composition using the pipette method and classified according to the USDA texture class thresholds, with the values 0.002, 0.05, and 2 mm (Blott & Pye, 2012) as upper limits for the clay, silt, and sand fractions, respectively. For all the samples, the soil organic carbon and the water content were also determined in the laboratory using standard protocols.

In Braccagni, the in situ acquisitions were carried out in June and July 2018, matching the hyperspectral airborne AVIRIS-NG acquisitions planned by ESA specifically for CHIME studies on 6 June 2018. The field was mainly plowed: only a subfield in the central part of the pivot was already sown; plants had already emerged in this part of the field with an average height of just a few centimeters. A stratified targeted sampling scheme based

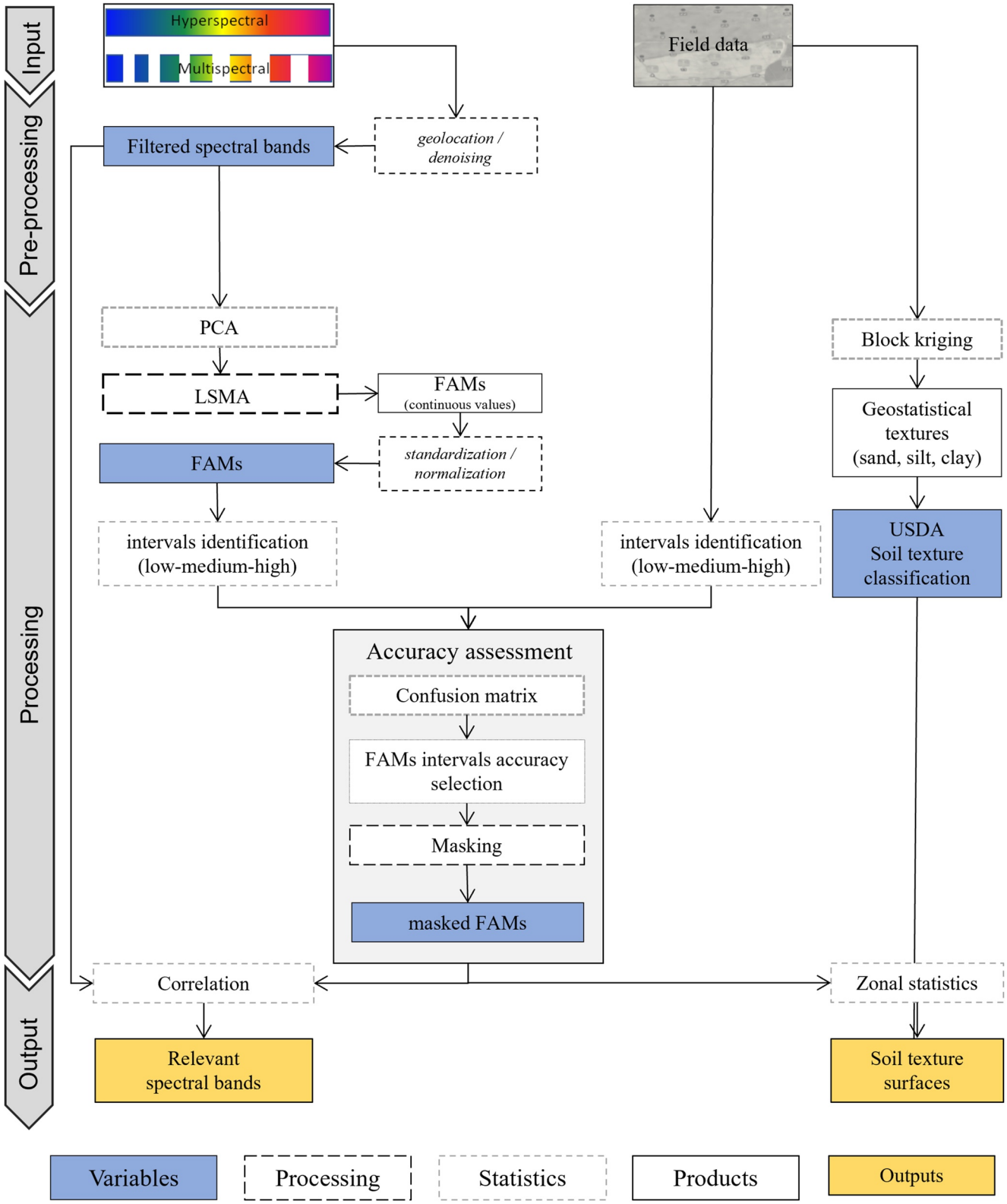

Figure 2. Workflow representing the processing chain and the output of the analyses. The acronyms stand for: LSMA—Linear Spectral Mixture Analyses; FAMs—Fractional Abundance Maps; USDA—United States Department of Agriculture.

Table 1
Technical Specifications of the Hyperspectral and Multispectral Sensors

Platform	CHIME	PRISMA	Sentinel 2 (A/B)	AVIRIS (airborne)
Sensor	CHIME	PRISMA	MSI	AVIRIS
Ownership	ESA	ASI	ESA	NASA JPL
Spectral bands and spectral ranges (nm)	210 bands (400–2,500)	VNIR: 66 bands (400–1,010) SWIR: 171 bands (920–2505) Panchromatic: 1 band (400–700)	VNIR: 10 bands (432–955) SWIR = 3 bands (1,359–2,289) 20 m (RedEdge, SWIR)	224 bands (365–2,550)
Spectral resolution (FWHM)	10 nm	≤12 nm	15–185 nm	10 nm
Spatial resolution	20–30 m	30 m (VNIR-SWIR) 5 m (Pan)	10 m (VNIR) 60 m (coastal aerosol, water vapor, cirrus)	3.6 m
Temporal resolution	10–12.5 days	29 days	5 days with two satellites	NA
Swath	–	30 km	290 km	11 km

on ancillary data and the LUCAS protocol was adopted for the selection of 95 samples distributed in Elementary Sampling Units (ESU) of 10 m. The pivot irrigation system was operating at the time of the AVIRIS acquisition (Figure 1).

In Maccarese, the in situ acquisitions were carried out on 11 November 2019, 28 January, and 17 February 2020, matching the hyperspectral satellite PRISMA overpasses tasked by the Italian Space Agency (ASI) specifically for PRISMA calibration and validation activities. Only completely bare soil fields were selected for field sampling, consisting of 97 ESU considering also some sub-ESU for better fitting the Sentinel 2 spatial resolution (Mzid et al., 2022). All the ESU were located in the central eastern units of the farmland (Figure 1).

2.2.2. Block Kriging

Since the soil ground sampling had a support size of about 4 m (bulked samples collected in a circle with 4 m diameter), the ground data could not be related to increasing resolution of the images, having pixel sizes of 20 and 30 m. Therefore, the spatialization of the in situ soil properties, using a block kriging technique, was carried out at the different spatial resolutions tested, that is, 3.6 m (as for the original AVIRIS NG airborne image's), 20 m (as for Sentinel's) and 30 m (as for CHIME-like's and PRISMA's). Both isotropic and anisotropic spherical variogram models were fitted to the experimental variogram, and the model chosen for the block kriging was selected on the basis of the cross-validation results using the Gstat package in R (Pebesma, 2004). A Box-Cox transformation was carried out to correct non-normality of the data and the fitting model selected was Matern, M. Stein's parameterization in all cases (Casa et al., 2020).

The textural designation determined from the block kriging provided three raster layers with the relative proportion of silt, clay and sand content. Following the USDA classification, those three layers have been classified into soil texture classes. The USDA system classifies soils into 12 soil texture classes represented using the ternary diagram (Davis & Bennett, 1927) with three broad primary textural groups of sand, silt and clay percentage. The USDA classification has been implemented using the Soil Texture Wizard Package (Moeys, 2018) in R environment obtaining discrete classes useful for a subsequent zonal statistical analysis.

2.2.3. Remote Sensing Data

Our analyses are based on the use of different hyperspectral data and the study of the synergies among different sensors, namely hyperspectral satellite data from the PRISMA mission (ASI), multispectral satellite data from the Sentinel 2 mission (ESA) and hyperspectral airborne data from AVIRIS-NG (NASA) resampled to CHIME and Sentinel 2 spatial and spectral features. The hyperspectral sensors, PRISMA and AVIRIS NG, similarly to CHIME, with more than 200 wavebands, cover the spectral range from 400 to 2500 nm with a spectral resolution of about 10 nm. PRISMA offers a spatial resolution of 30 m in the VNIR-SWIR spectral region, and it is quite comparable with CHIME, which should have a target spatial resolution between 20 and 30 m. The MultiSpectral Instrument (MSI) sensor onboard Sentinel 2 offers 13 wavebands in the VNIR and SWIR and the potential for data fusion to leverage the spectral resolution of hyperspectral sensors and the spatial and temporal resolution of multispectral constellations (Table 1).

As part of the CHIME RCS project, ESA, during the year 2018, funded specific airborne hyperspectral acquisitions with AVIRIS-NG as a mission performance simulator. The image that captured the Braccagni area on 21 June 2018 has been used in our analyses since it represents a good compromise between low cloud cover and the extensive presence of bare soils within the farm. AVIRIS-NG data on Braccagni farm was corrected from the atmospheric and water vapor effect directly from the provider and for this study, it was resampled following a CHIME-like (30 m, 211 bands) and S2-like (20 m, 13 bands) configuration.

PRISMA and Sentinel 2 data were used as hyperspectral and multispectral input data in Maccarese. PRISMA image that captured the Maccarese farmland on 2022 was acquired

Table 2
Input Images Used

Study site	Sensor	Date	Cloud coverage	Noisy bands
Braccagni	AVIRIS-NG CHIME-like	21 June 2018	0%	Removed 26/211: SWIR: 1,379.5–1,439.5 (99–105), 1,809.5–1,929.5 (142–154), 2449.5–2498.6453 (206–211)
	AVIRIS-NGS2-like	21 June 2018	0%	–
Maccarese	PRISMA	14 July 2022	0.005%	Removed: 93/234
				VNIR: SNR low: 402.4–463.7 (1–9)
				Bands with random spike: 770.5 (44); 913.4 (57); 944.6 (60); 967.0 (62)
				Bands in overlapping zone: 929.3 (59); 951.3 (61); 972.6 (63)
				SWIR: Bands in overlapping zone: 942.9–998.4 (3–9)
				Bands with random spike: 1,120.7–1,196.2 (21–28); 1,553.8–1,544.2 (59–60); 1,803.6 (86)
				Atmospheric water absorption: 1,328.1–1,522.9 (40–58); 1,812.8–2052.7 (87–114)
				SNR low 2420.9–2496.9 (162–173)
	Sentinel 2	14 July 2022	1.7%	Removed 1/13: 1,373.5 (10)

Note. In the Noisy bands column, the removed bands are expressed in wavelengths in nm and with the original band number (enclosed in brackets).

from the ASI catalog client (https://prisma.asi.it/) in the Hierarchical Data Format–Earth Observing System 5 (HDF-EOS5) with pre-processed Level 2C (ground reflectance without geometric correction). Sentinel 2 image was acquired from Theia catalog (https://www.theia-land.fr/en/typeofproduct/sentinel-2/) in Level 2A, which are corrected from the atmospheric effects using the MACCS-Atcor Joint Algorithm (MAJA).

2.2.4. Pre-Processing

The AVIRIS-NG image that captured the Braccagni farmland on June 2018 was resampled into a CHIME-like image with 211 bands and 30 m spatial resolution using the CHIME's spectral and spatial configurations. The image was also resampled to the 13 Sentinel 2 spectral bands and to a spatial resolution of 20 m to obtain a Sentinel 2-like configuration.

A Gaussian spectral resampling model was used, based on the spectral response function (SRF) provided by ESA for both CHIME and Sentinel 2 and by using an ASCII wavelengths file containing the full-width-half-maximums (FWHM) for each band. The spatial resampling from 3.6 m resolution to 30 and 20 m was performed using a Nearest Neighbor algorithm implemented in ENVI 5.5.2. software (L3Harris Technologies). To complete the pre-processing steps of the AVIRIS data set, the noisy bands affected by atmospheric water absorption have been removed from the SWIR wavelengths (Table 2).

The Level 2-C PRISMA images were corrected by the residual geospatial shift (related to lack of the Ground Control Points within the standard geocoding process), using the contemporary acquired Sentinel 2 images as references for orthorectification in ENVI 5.6 PRISMA toolkit (L3Harris Geospatial Technologies). Before merging PRISMA VNIR and SWIR hyperspectral band set into a single layer stack, it was needed to remove the overlapping reflectance bands in the 930–998 nm spectral range and the removal of bands affected by atmospheric water absorption noise (Table 2). Few more bands determining spikes effects in the spectral signatures and having stripes were also removed manually. Finally, the band removal related to Signal to Noise Ratio (SNR) was manual and based on the rising of SNR from green (≈200) to far-red (≈400) and NIR-SWIR (≈500), with the lowest values at wavelengths larger than 2000 nm (≈100) (Table 2) (Cogliati et al., 2021).

2.2.5. Linear Spectral Mixture Analysis

The hyperspectral and multispectral data were used to identify topsoil texture classes following the USDA classification. The application of a sub-pixel analysis technique was based on the consolidated approaches proposed by

Boardman (1995), Sousa and Small (2018), and Valentini et al. (2020). Several approaches have been developed for determining the relative value of individual endmembers for representing the spectral variability captured by an image. In our approach, the endmembers (EMs) selection is based on the analysis of the multi-dimensional space obtained with the Principal Component Analysis (PCA) of each spectral configuration (CHIME-like, PRISMA and Sentinel) after noisy band removal.

With the Principal Component Analysis (PCA) we first obtained the reduction of the dimensionality of the hyperspectral bands by projecting them into N orthogonal directions or eigenvectors (PCs). Second, the EMs selection was obtained in correspondence with the orthogonalized pixel clouds by exploring the spatial distribution of the pixels in two-dimensional PCs mixture spaces (2D scatterplots). The manual selection of the EMs in the two-dimensional PCs mixture space is an expert based image-based extraction of the spectral variance captured by each pixel (Plaza et al., 2002).

To overcome the uncertainties related to the variation of the spectral signal within each endmember collection, we assumed that there are not differences in illumination within the field unit captured by the images since both croplands are in relatively flat areas and hence the only difference between image pixels reflectance could be in terms of moisture. We also assumed that in cultivated soils, due to repeated tillage operations, soil properties, including texture, organic content and mineralogy, are usually quite uniform over the tilled layers; therefore they can be estimated from the bare soil surface reflectance (Casa et al., 2013). After performing the unconstrained unmixing, to have sets of fractional maps representing the linear abundance percentage in each pixel, first, a standardization of values from 0 to 1 has been applied. As second step, a sum constraint to 1 was applied implementing a simple proportion using the FAMs as a pixel's data frame and by dividing the columns by the sum of the rows (Equation 1).

$$X_{i,j}\mathrm{norm} = \frac{X_{i,j}}{\sum_{k=1}^{n} X_{i,j}} \tag{1}$$

where

X = FAMs value.

i, j = FAMs.

n = FAMs number.

2.2.6. Accuracy Assessment

The last step of the LSMA was the validation of FAMs through the confusion matrix technique using the field data. Both the field data and the FAMs were classified into three intervals following the general criteria of equal breakdown distribution. For the FAMs, as a consequence of the standardization and normalization, values were ranging from 0 to 1 with different maximum values and some empirical adjustment was introduced to redefine the interval limits. The intervals identified with this thresholding method, offered the opportunity of validating the overall accuracy of each FAM on the base of the ground truthing data (i.e., soil textures). Moreover, this confusion matrices, provided an estimate of the accuracy of each FAMs interval with specific ground truthing texture interval highlighting the potential amount of each texture class captured by FAMs. A total of 36 confusion matrices has been computed (2 sites × 2 sensors × 3 FAMs × 3 intervals). Once defined the accuracy for each interval, the less accurate part of each FAM has been removed by masking.

2.2.7. Zonal Statistics

A comparative analysis to test the spatial patterns of USDA kriging-based classifications and each masked-FAM was performed exploiting a zonal statistics operation. The zonal statistics, follow a raster-based method where the zones are defined by USDA textural classes while the statistics comes from masked-FAMs value. It returns as output, a table where the overlapping zones are reported in terms of surfaces and number of pixels, allowing the attribution of each masked-FAM to the different USDA textural classes.

2.2.8. Relevant Spectral Bands

To exploit the LSMA results in understanding the performances of different spectral wavelengths' ranges with respect to the detection of soil texture classes, correlation matrices, including as input variables the masked-FAMs and wavebands of each sensor, have been implemented. The linear Bravais-Pearson correlation between

Table 3
Braccagni Field Sample Basic Statistics

	Clay	Silt	Sand	SOC
Mean	26.83	54.96	18.21	1.36
Standard error	0.70	0.63	0.63	0.02
Median	26.20	55.60	17.20	1.34
Standard deviation	6.81	6.15	6.14	0.15
Variance	46.31	37.88	37.73	0.02
Kurtosis	−0.15	−0.16	−0.27	0.28
Skewness	0.33	−0.45	0.49	0.12
Range	31.60	28.60	27.20	0.79
Minimum	12.30	38.70	7.70	0.93
Maximum	43.90	67.30	34.90	1.72
Count	95	95	95	95

the variables was analyzed with regard to the sign (i.e., positive or negative) and the magnitude (i.e., values from −1 to 1).

3. Results

The results description follows the workflow presented in Figure 2. To ease readability, a selection of the most relevant results is presented hereunder for each of the two study areas and for each sensor configuration whereas all the processing results are reported in the Supporting information.

3.1. Braccagni Farmland: CHIME-Like Data Set

3.1.1. Field Variability

The 95 field samples over the farmland provided the proportion of sand, silt and clay expressed as texture percentages. The most abundant texture over the whole area was silt, resulting in minimum and maximum values of 38.70% and 67.30%, followed by clay with 12.30% and 43.90%, and sand with 7.70% and 34.90%. The respective averages were 54.96%, 26.83%, and 18.21% (Table 3).

3.1.2. USDA Soil Texture Classification

The block kriging technique was applied to the entire set of field measurements obtaining robust estimations of the topsoil properties for the two spatial resolutions, namely 30m for fitting CHIME-like and 20m for Sentinel 2-like (Figure 3). The block kriging estimation maps of sand, silt and clay were based on variogram models resulting similar for silt and clay. These two models were also very similar to the one provided by the soil organic carbon content (Figure S1 in Supporting Information S1).

The USDA soil classification thresholds applied to the estimation maps of clay, silt and sand provided five USDA texture classes. With this classification, the soil of the area resulted dominated by clay loam and loam classes. Only in the southern-west part there was a higher abundance of the Clay class (Figure 3).

3.1.3. Linear Spectral Mixture Analyses

In the multidimensional space identified by the first two or three Principal Components (PCs'), through the manual apex's selection of the 2D scatterplots, four EMs were identified. The spectral profiles of EM1, EM3 and EM4 of CHIME-like and Sentinel 2-like were associated with topsoil typologies. The two sensor configurations identified similar EMs collections with a bundle of spectral signatures of comparable shape differing mostly in terms of intensities. EM2 has been associated to the soil moisture absorption effect having the lowest reflectance values (<0.01) even with a typical soils shape (Figures 4a–4d).

In CHIME-like configuration, the LSMA has a RMSE of 0.23 and the abundance maps, FAM1 and FAM3, have a spatial pattern recognizing the presence of two complementary areas where values of FAMs are around 60%. In Sentinel 2-like data, the mean RMSE is of 0.13 and FAM1, which shows values greater than 40% in the central

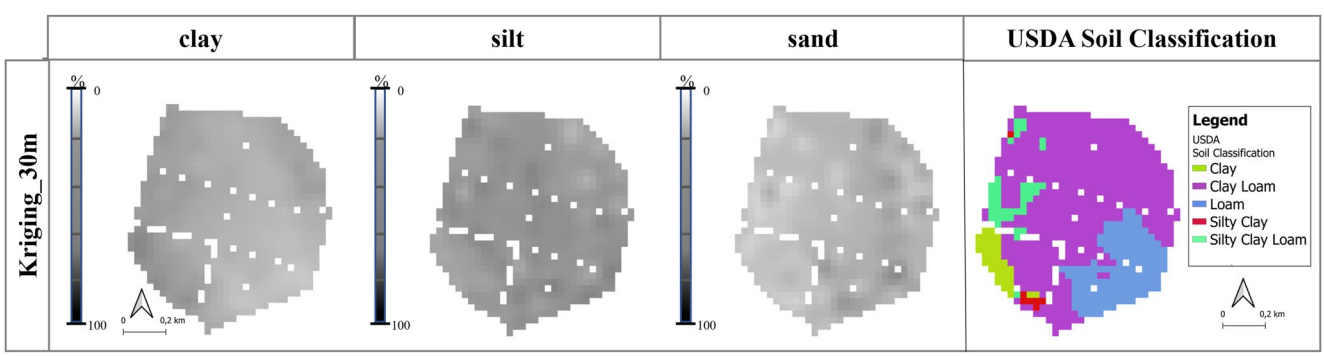

Figure 3. Estimation maps of clay, silt and sand obtained by applying block kriging for the Braccagni farmland. The last map represents the USDA Soil Texture Classification based on estimation maps.

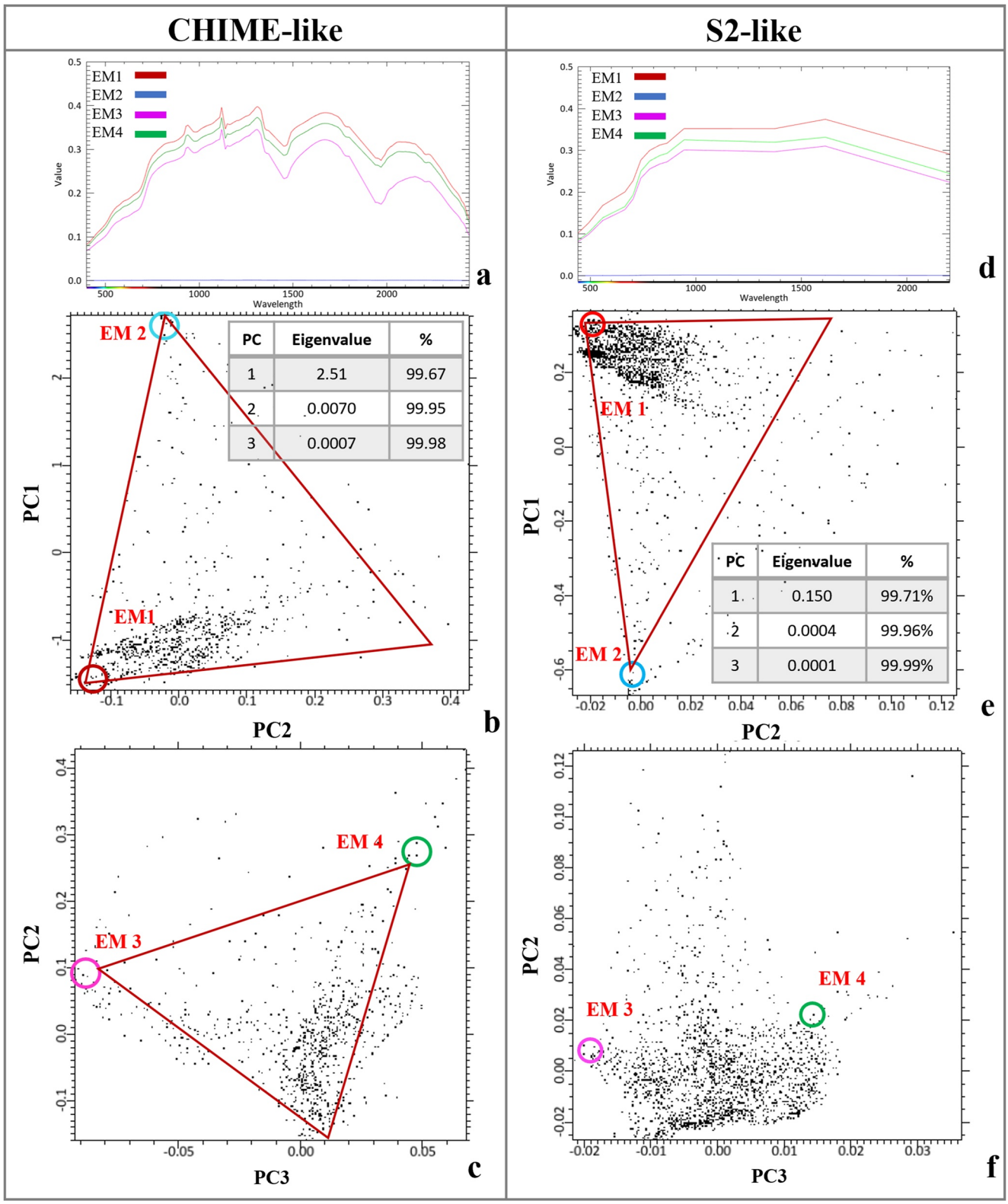

Figure 4. Endmembers (EMs) collection and position in the multidimensional space for CHIME-like (left, a–c) and Sentinel 2-like (right, d–f). Red lines are used to facilitate the readability of the 2D scatterplots' shape; the circles are to identify the position of the EMs and the color of the circles on the scatterplots correspond to the color of the EMs in the spectral graphs (a and d).

Table 4
Thresholds Used for Validation Purposes

	Field thresholds			CHIME-like thresholds			Sentinel 2-like thresholds		
Class	Clay	Silt	Sand	FAM1	FAM3	FAM4	FAM1	FAM3	FAM4
Low	<15	<40	<10	<0.2	<0.2	<0.2	<0.2	<0.15	<0.15
Medium	15–30	40–60	10–20	0.2–0.45	0.2–0.45	0.2–0.45	0.2–0.4	0.15–0.3	0.15–0.3
High	>30	>60	>20	>0.45	>0.45	>0.45	>0.4	>0.30	>3

portion of the pivot, has a similar spatial pattern to the FAM1 of CHIME-like. FAM2 and FAM4 show lower fractional cover values (<40%) and lower spatial variance over the area for both configurations (Figure S2 in Supporting Information S1).

3.1.4. Accuracy Assessment

The retrieval accuracy is based on the overall accuracy (OA) and the producer accuracy (PA) obtained with the confusion matrix between all ground truthing field sample and FAMs. Both datasets have been classified into three classes by thresholding their distributions in three abundance intervals: low, medium and high. All the thresholds are reported in Table 4. For both the configurations FAM2 has been excluded from the validation data set because it has been associated with the moisture-darkness effect.

Considering the CHIME-like configuration, the FAM3 has the highest OA (41.3%), mostly determined by the class medium sand (PA = 43.24%). Similarly, FAM1 shows high OA (39.1%) determined by the class high sand (PA = 86.5%), while FAM4 presents the lowest values of OA (27.2%) determined by the class medium silt (PA = 36.2%).

In Sentinel 2-like configuration, FAM4 shows the lowest accuracy and all the FAMs show the highest OA for silt with different intervals. The FAM3 has the highest OA (55.8%), mostly determined by the class medium silt (PA = 68.6%). FAM1 shows high OA (45.3%) determined by the class high silt (PA = 86.5%) while FAM4 presents the lowest values of OA (35.7%) determined by the class medium silt (PA = 48.6%) (Table S1 in Supporting Information S1). Considering all the validation results, CHIME-like configuration provided a wider set of validated FAMs than Sentinel 2-like. The multispectral resolution was in fact accurate only with silt (Data Set S1).

The confusion matrix results have been used to set the intervals deemed suitable for texture classes (i.e., USDA soil texture classification) retrieval (Figure 5).

3.1.5. Soil Texture Surfaces

The zonal statistics allowed to retrieve from each FAM the overlapping zones with the different classes of the kriging-based USDA map (Table 5). In CHIME-like, FAM1 > 0.45 covers the 50% of the study area and the greatest overlap is with the clay loam class (86%). Also the FAM4 0.20–0.45, that covers only the 22% of the study area, is overlapping for the 66% of its surface, the clay loam class. The FAM3 > 0.45 is the smallest in terms of surface and it overlaps almost the loam class (70%). Since both FAM1 and FAM3 are validated by class high sand (20%–35%) from the confusion matrix, it is reliable that the attribution of FAMs to texture classes are the proportion of silt and clay. In fact, according to the USDA intervals, there are similar sand values in the loam class (52% or less) and clay loam (45% or less), while they differ in the amount of clay (7%–27% in Loam, 27%–40% in Clay Loam) and silt (28%–50% in Loam) (Ditzler et al., 2017).

In the Sentinel 2-like configuration, the zonal statistics provided different FAMs overlap with the USDA texture classes compared to the CHIME-like. Both FAM1 > 0.40 and FAM3 0.15–0.30 show the majority of surface overlapping the Silty Clay class. The FAM4 0.15–0.30 covers about the 50% of the USDA map and it overlaps the Clay class for the 32%. The driver soil property is silt as already verified with the confusion matrix, because in the USDA thresholds, silt is present with different percentages in Silty Clay (40% or more) and in Clay (40% or less). In fact, from the confusion matrix, FAM1 is validated with high values (>60%) of silt, while FAM3 with medium values (40%–60%).

3.1.6. Relevant Spectral Bands

Spectral correlation between the relevant masked FAMs and the original wavebands of each sensor configuration (i.e., CHIME-like and Sentinel 2-like) provided some ranges of spectral wavelengths of high correlation.

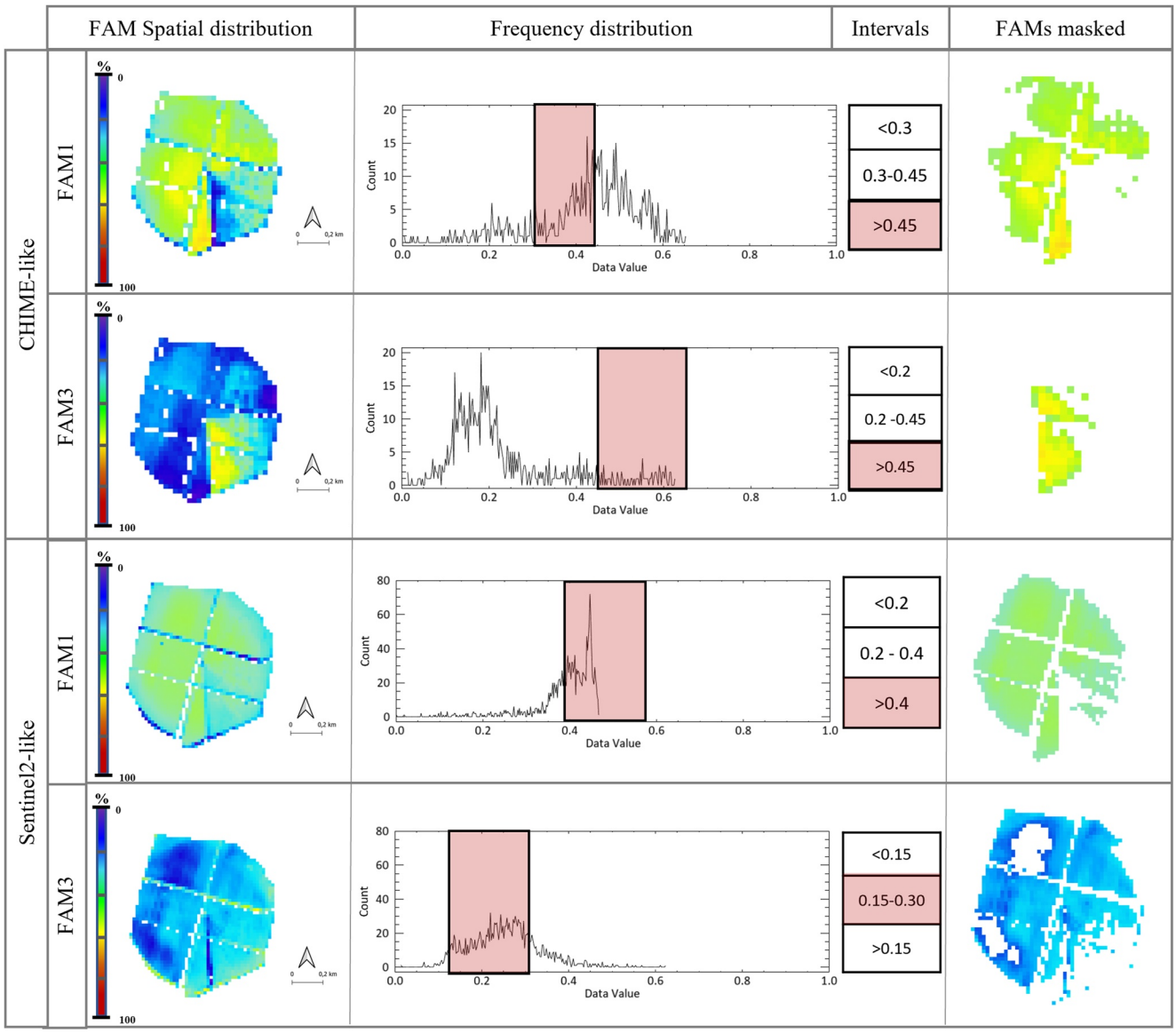

Figure 5. Summary table of the suitable intervals selected for masking FAMs values in the Braccagni area. In the last column the FAMs are masked on the base of the intervals obtained by the validation and represented with the red highlight on the histogram.

CHIME-like FAM1 > 0.45 shows in the VIS wavelength range of 509–709 nm, an average correlation value of 0.45. This value is lower than Sentinel 2-like FAM1 > 0.40, which reaches an average of 0.85. With the SWIR spectral region, we observed two areas of high correlation: in the wavelength range of 1,449–1,609 nm, the average correlation value is 0.65 for CHIME-like FAM1 > 0.45 and is 0.68 for Sentinel 2-like FAM1 > 0.40; in the wavelength range of 1,939–2,019 nm, the average correlation value is 0.85 for CHIME-like FAM1 > 0.45 and is 0.78 for Sentinel 2-like FAM1 > 0.40 (Figure 6) (Data Set S2).

3.2. Maccarese Farmland: PRISMA Data Set

3.2.1. Field Variability

The field samples analysis provided the percentage of different topsoil properties resulting in minimum and maximum values for clay of 18.37% and 50.24%, silt of 14.16% and 38.32% and sand of 23.10% and 64.42%, with the respective averages of 37.16%, 25.29%, and 37.55%. The highest abundance was observed for sand over the whole area (Table 6). The block kriging technique was applied to field measurements to obtain clay, silt and sand estimation maps (Figure 7).

Table 5
Zonal Statistics of Masked FAMs and Kriging-Based USDA Classification

CHIME-like	USDA	FAM1 > 0.45		FAM3 > 0.45		FAM4 0.20–0.45	
Class	m^2	m^2	%	m^2	%	m^2	%
Clay	32,400	2,700	1	–	–	22,500	14
Clay loam	498,600	304,200	**86**	18,000	29	103,500	**67**
Silty clay	6,300	3,600	1	–	–	6,300	4
Silty clay loam	37,800	25,200	7	–	–	2,700	2
Loam	137,700	16,200	5	43,200	71	20,700	13
Sentinel 2-like	**USDA**	**FAM1 > 0.40**		**FAM3 0.15–0.30**		**FAM4 0.15–0.30**	
Class	m^2	m^2	%	m^2	%	m^2	%
Clay	147,600	58,800	14	99,200	21	11,400	**32**
Clay loam	172,400	126,400	**30**	111,200	**24**	90,000	25
Silty clay	237,200	133,200	**32**	145,600	**31**	78,400	22
Silty clay loam	48,000	35,200	8	46,400	10	45,200	13
Loam	40,800	34,800	8	29,600	6	19,200	5
Silty loam	80,800	32,400	8	36,800	8	12,400	3

Note. The bold values indicate the highest overlapping surfaces.

3.2.2. USDA Soil Texture Classification

The distribution of the soil properties is homogeneous throughout the area with a more abundant presence of sand in the north-east than of silt or clay. However, silt is the less represented soil property while the sand is the most abundant. The USDA Soil Texture Classification applied to the block kriging estimates has provided a thematic map characterized by three texture classes: the area is mostly represented by the clay loam class, while in the central part there are zones with Clay class and in the north-eastern part there is a small area characterized by the sandy clay loam class (Figure 7).

3.2.3. Linear Spectral Mixture Analysis

The multidimensional space of PRISMA and Sentinel 2 provided a bundle of three EMs for each sensor. The spectral signatures of both spectral configurations were associated to a typical soil spectral profile. In PRISMA, EM1 and EM3 have a similar shape differing only in the reflectance intensity. The spectral profile of EM1 and EM3 change in intensity values over 1,400 nm, showing an inversion of the relative positions (Figure 8a).

The spectral profiles of EM1 and EM3 in Sentinel 2 have similar shapes with small differences in the absorption features in the NIR-SWIR wavelengths. EM2 has the lowest intensity (reflectance < 0.40) for both sensors, but in Sentinel 2 the shape of the spectral profile in the red edge could suggest the presence of sparse senescent vegetation.

For PRISMA, the LSMA with a mean RMSE of 0.17, retrieved FAM1 as the most representative in terms of cover percentage (>60%). The FAM2 presents lower coverage values between 30% and 50% and shows a distribution of fractional abundances complementary to FAM1. Although FAM3 presents low values of fractional coverage over the whole area, this fraction identifies two different zones in the farmland unit with higher values in the northern portion reaching 50% (Figure S3 in Supporting Information S1). This zonation could be associated to the presence of sparse residual Non Photosynthetic Vegetation (NPV) in the northern portion.

In the Sentinel 2 image, acquired on the same day of PRISMA acquisition, the RMSE was 0.1. The FAMs retrieved with multispectral configuration do not show significant patterns in the fractional abundance even if FAM1 has values >50% on the whole area. What appears evident in all the FAMs, are the alternating parallel stripes of low and high cover values. As in PRISMA retrieval, FAM3 identifies two distinct areas that could be explained, given the signature of the EM3, with the presence of dead vegetational residues in the southern portion (Figure S3 in Supporting Information S1).

3.2.4. Accuracy Assessment

The retrieval accuracy is based on the confusion matrix between the ground truthing field sample and FAMs. Of the 97 samples for computing the validation, only 92 have been selected because some of them overlapped the border of the farmland unit. Both datasets, FAMs and field, were classified by thresholding their distributions in three abundance intervals: low, medium and high. All the intervals are reported in (Table 7).

Considering the PRISMA configuration, the FAM2 has the highest OA (45,5%), mostly determined by the class medium sand (PA = 66%).

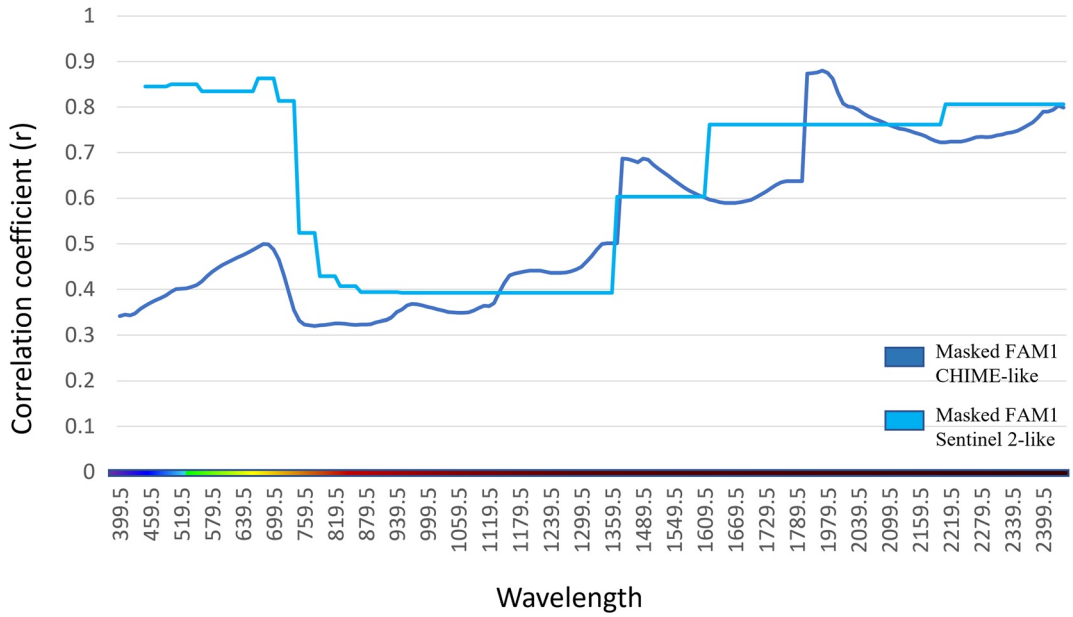

Figure 6. In blue correlations of CHIME-like FAM1 > 0.45 and the 185 CHIME-like spectral bands (wavelengths); in cyan correlation of Sentinel 2-like FAM1 > 0.40 and the 12 Sentinel 2-like spectral bands.

FAM1 shows an OA (42.4%) determined by the class high silt (PA = 48.8%), while FAM3 presents the lowest values of OA (23.3%) determined by the class low sand (PA = 68.8%).

In Sentinel 2 configuration, as happen in PRISMA, the FAM1, the one with the highest OA (52.7%), is mostly influences by the class high silt (PA = 80%). FAM2 shows high OA (47.8%) determined by the class medium clay (PA = 62.2%) (Table S2 in Supporting Information S1) (Data Set S1).

The confusion matrix results have been used to set the intervals deemed suitable for soil texture surfaces (i.e., USDA soil texture classification) analyses (Figure 9).

3.2.5. Soil Texture Surfaces

In the PRISMA configuration all the FAMs show the greatest overlap with the clay loam class with surface areas of 61% for FAM1 > 0.5, 63% for FAM2 0.20%–0.35% and 62% for FAM3<0.20 (Table 8).

The same observation is made for the Sentinel 2 configuration in which all the masked FAMs cover the majority of the study area and overlap clay loam class with surfaces of 56%.

In PRISMA the spatial patterns of FAM1 > 0.5 and FAM2 0.20–0.35 could be associated respectively to fine and coarse texture classes. In particular FAM1 > 0.5 on medium values was validated by high silt class (25%–38%) conversely, medium values of FAM2 0.20–0.35 were validated by medium sand class (30%–40%) fitting the clay loam USDA class (27%–40% clay 20%–46% sand). For Sentinel 2 considering the high spatial resolution it is evident the effect of the stripes, probably due the geometry of the plowing practices.

Table 6
Field Sample Basic Statistics of Maccarese Farmland Unit

	Clay	Silt	Sand
Mean	37.16	25.29	37.55
Standard error	0.69	0.46	0.86
Median	37.08	25.91	35.93
Standard deviation	6.82	4.50	8.48
Variance	46.47	20.25	71.83
Kurtosis	0.08	0.33	1.12
Skewness	−0.29	−0.20	1.02
Range	31.87	24.17	41.31
Minimum	18.37	14.16	23.10
Maximum	50.24	38.32	64.42
Count	97	97	97

3.2.6. Relevant Spectral Bands

Spectral correlations between the relevant masked FAMs and original wavebands of each sensor configuration (i.e., PRISMA and Sentinel 2) provided similar results to CHIME-like and Sentinel 2-like for the SWIR wavelength range. PRISMA FAM1 > 0.5 shows in the VIS wavelength range, negative average correlation value of −0.35 while Sentinel 2 > 0.5 has positive but very low correlation (0.12). Both sensors have the highest positive values

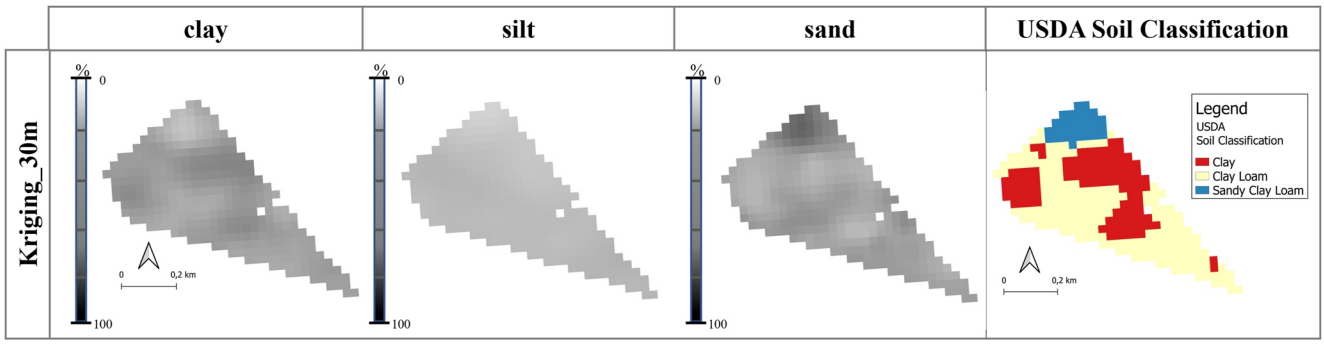

Figure 7. Estimation maps of clay, silt, and sand obtained by applying block kriging for the Maccarese farmland. The last map represents the USDA Soil Texture Classification based on estimation maps.

for the SWIR wavelengths over 1,500 nm, but PRISMA correlations are higher than Sentinel 2. Considering the nearest spectral range of high correlation obtained with CHIME-like FAM1 > 0.4 (1,449–1,609 nm, $R = 0.65$; 1,939–2019 nm, $R = 0.85$) in the SWIR, with PRISMA FAM1 > 0.5, for wavelength range of 1,554–1,616 nm, the average correlation value is 0.74 and for wavelength range of 1,784–2061 nm is 0.68. It has to be noted that

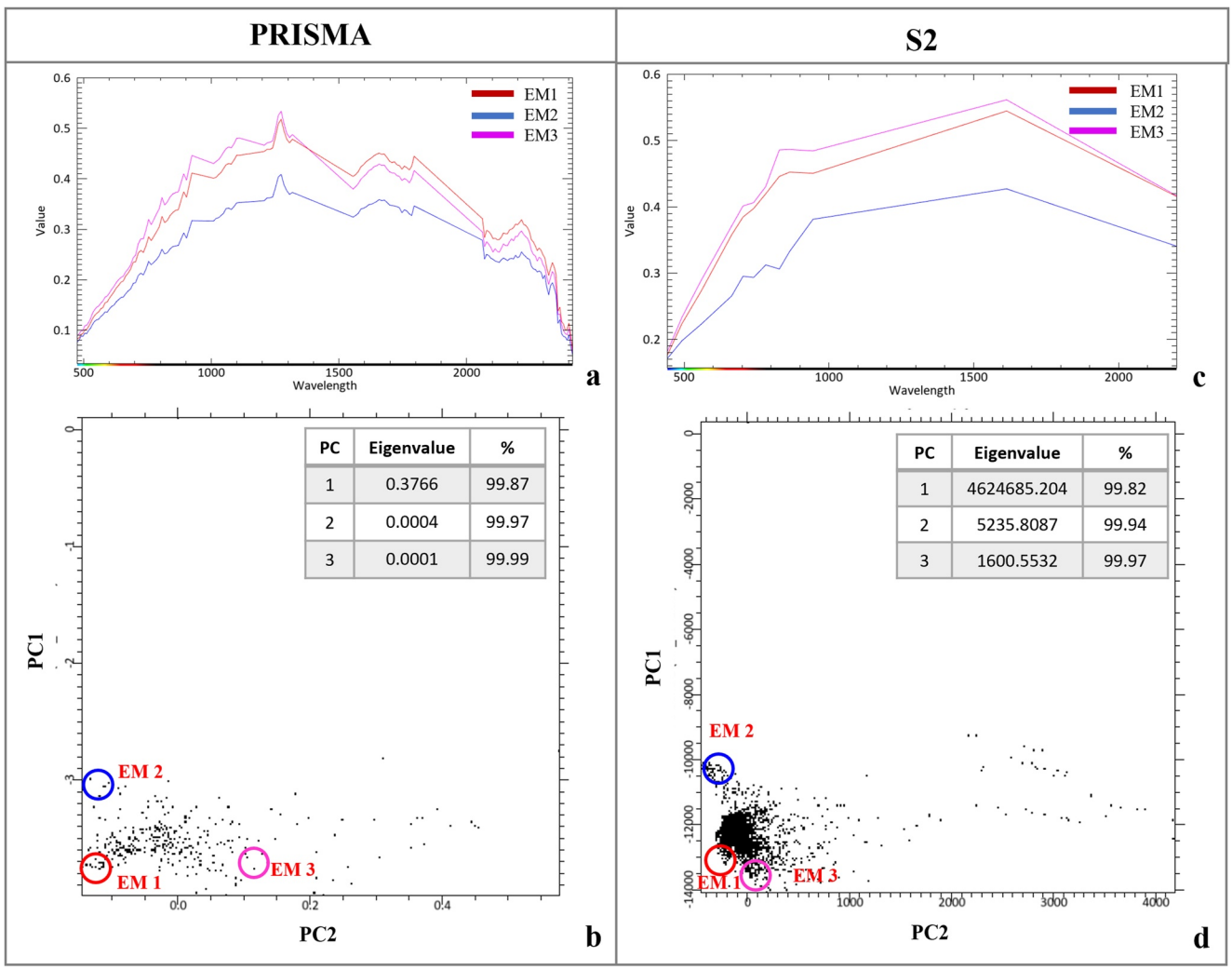

Figure 8. Endmembers (EMs) collection and position in the multidimensional space for PRISMA (left, a and b) and Sentinel 2 (right, c–f). The circles are to identify the position of the EMs and the color of the circles on the scatterplots correspond to the color of the EMs in the spectral graphs (b and d).

Table 7
Thresholds Used for Validation

	Field thresholds			CHIME-like thresholds			Sentinel 2-like thresholds		
Class	Clay	Silt	Sand	FAM1	FAM3	FAM4	FAM1	FAM3	FAM4
Low	<30	<20	<30	<04	<0.2	<0.2	<0.3	<0.2	<0.3
Medium	30–40	20–25	30–40	0.4–0.5	0.2–0.35	0.2–0.4	0.3–0.5	0.2–0.4	0.3–0.5
High	>40	>25	>40	>0.5	>0.35	>0.4	>0.5	>0.4	>0.5

in the wavelength range from 1939 to 2019 nm, CHIME-like FAM1 > 0.4 shows a peak of correlation but in PRISMA spectral bands of this range were removed after noisy band filtering (Figure 10).

The negative correlations are probably due to the presence of some dry vegetation laying on the bare soils and to the presence of small irrigation channels (width < 30 m), paths and vegetated edges in the field unit. Further, the

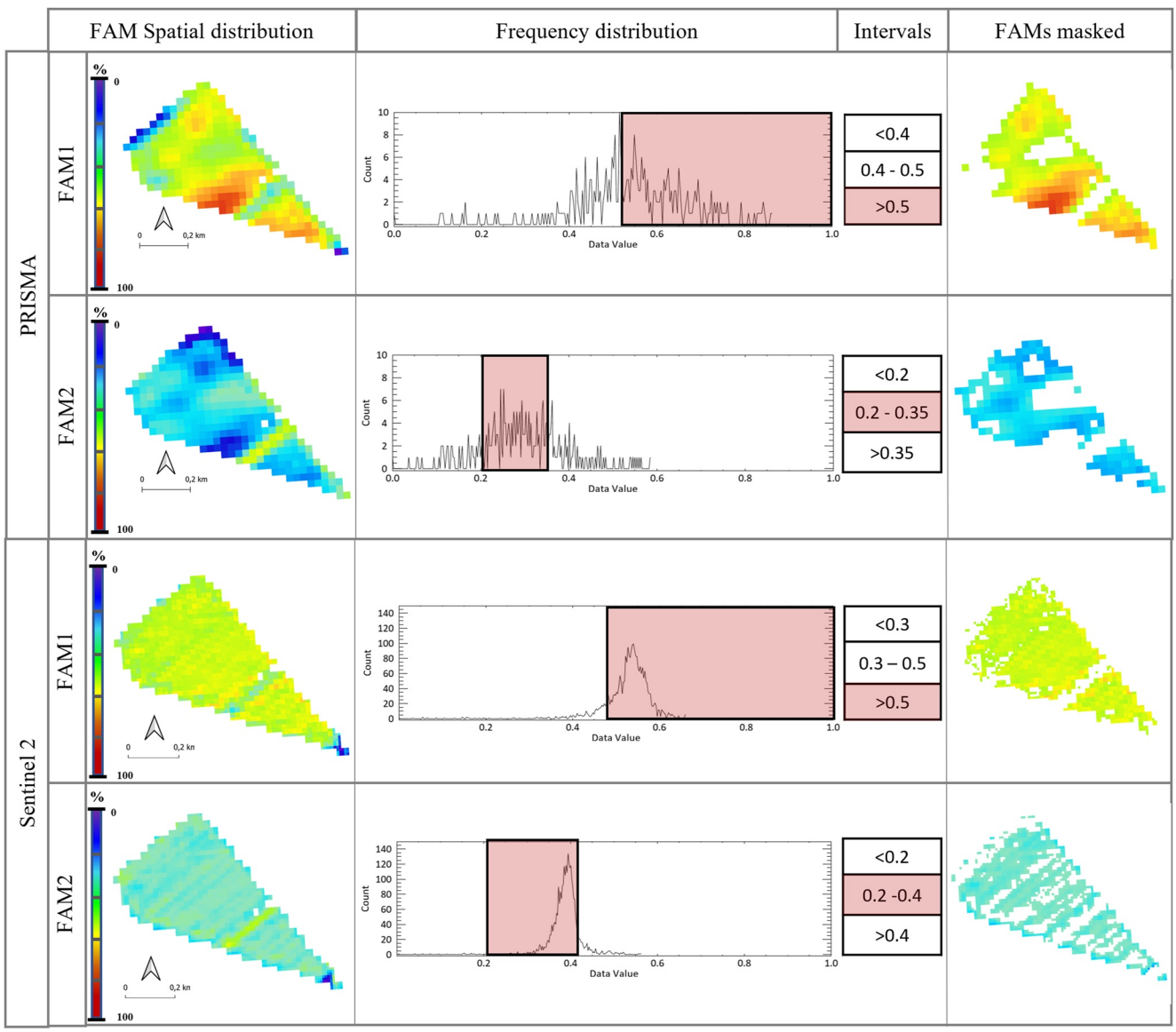

Figure 9. Summary table of the suitable intervals selected for masking FAMs values in the Maccarese area. In the last column the FAMs are masked on the base of the intervals obtained by the validation and represented with the red highlight on the histogram.

Table 8
Zonal Statistics of Masked FAMs and Kriging-Based USDA Classification

PRISMA	USDA		FAM1 > 0.5		FAM2 0.20–0.35		FAM3 0–0.20	
Class	m^2		m^2	%	m^2	%	m^2	%
Clay	89,416		52,142	28	47,096	30	68,121	34
Clay loam	155,585		111,853	61	98,397	63	125,309	62
Sandy clay loam	26,071		19,343	11	11,774	7	9,251	4
Sentinel 2	**USDA**		**FAM1 > 0.5**		**FAM2 0.20–0.40**		**FAM3 < 0.20**	
Class	m^2		m^2	%	m^2	%	m^2	%
Clay	91,200		77,700	36	63,700	35	91,100	35
Clay loam	155,300		120,400	56	101,700	56	148,700	56
Sandy clay loam	24,700		19,400	9	16,700	10	24,600	9

unit is divided into two subareas with different reflectance, as can be seen from all the FAMs spatial patterns (Figure 9) (Data Set S2).

4. Discussion

The main goal of the present work was to test the potential of hyperspectral data for the detection of topsoil texture properties with linear spectral unmixing models. Soil texture is an important property related to physical, chemical and biological soil processes, and the potential of soil texture thematic mapping in relation to the development of the Copernicus Land Monitoring Service is one of the main goals to be reached with the upcoming hyperspectral Copernicus satellite mission (CHIME), a mission that will be capable of imaging agricultural areas globally and at a regular cadence. Hyperspectral imaging for topsoil properties prediction has very limited applications outside research but with the new sensors' generation, it could be a valid support for image-based detection.

The analyses presented assume that, for bare soils agricultural units, the physical variability of reflectance mixtures captured by an image could depend on (a) the soil moisture and organic matter content, that generally determine absorption effects; or (b) the slightly variation of soil textures classes distributions within the unit. These statements are based on the idea of having homogenous mineralogical composition within single agricultural units because of the continuous plowing that makes soils well mixed.

The use of a image data point model for the EMs estimation based on the PCA to orthogonalize bands, allows the estimation of mixtures within pixels using only the mixed data themselves. The EMs selection based on the concepts of convex geometry allows the linear mixture problem to be treated using the linear inverse theory (Boardman, 1995), and the formal definition of the EMs, corresponds to the vertices of a convex set that covers the image data. To further understand the validity of this method it is necessary the exploration of other case studies and to test unsupervised methods of EMs selection. The critical step of determining the EMs used as the references for the unmixing process is widely discussed in literature for large scale datasets (Veganzones & Graña, 2008) but basically the transformation of the image data are the predominant techniques. The relationship between spectral responses and the chance of scaling the method to large areas could of course be affected by strong non-linearities due to the involvement of multiple factors. The retrieval results of this study are in fact, even with good accuracy for some FAM interval, constrained by (a) the low variability identified with only two case studies; (b) by the manual expert based selection of the EMs; (b) the empirical thresholding of FAMs intervals.

In Braccagni, CHIME-like configuration provided a wider set of validated FAMs than Sentinel 2-like, and the multispectral resolution resulted accurate only with medium and high silt intervals. In CHIME-like, FAM1 > 0.45 has the greatest overlap with the clay loam class (86%) and both FAM1 and FAM3 are validated by high sand class (20%–35%) revealing that the two are detecting the relative proportions of silt and clay. Indeed, dark soils, soil moisture content and parental material generally contain higher clay and lower sand than soils with light shades, with greater presence of sand (Castaldi et al., 2016; Viscarra Rossel et al., 2011, reported that the estimate of silt from spectral data is less accurate than that of clay and sand. This is a consequence of its variability, generally much smaller than that of the other two classes. However, they suggest that, in a practical situation, silt can better be obtained as a complement to 100 of the other soil fractions rather than with an independent estimate. Thus, it must be considered that the Braccagni farmland is characterized by a homogeneous spatial distribution of silt, which made it difficult to capture its contribution to the spectral variability of each pixel. Moreover, in this area, the best spectral performances of Sentinel 2-like configurations are only for the VIS wavelengths (r = 0.85) where the multispectral has most of the bands and the highest spatial resolution. In the SWIR wavelengths instead, average values of correlation coefficient for CHIME-like are higher than the Sentinel 2-like (Figure 6) in accordance with Casa et al., 2013; Castaldi et al., 2016; Gholizadeh et al., 2018 studies.

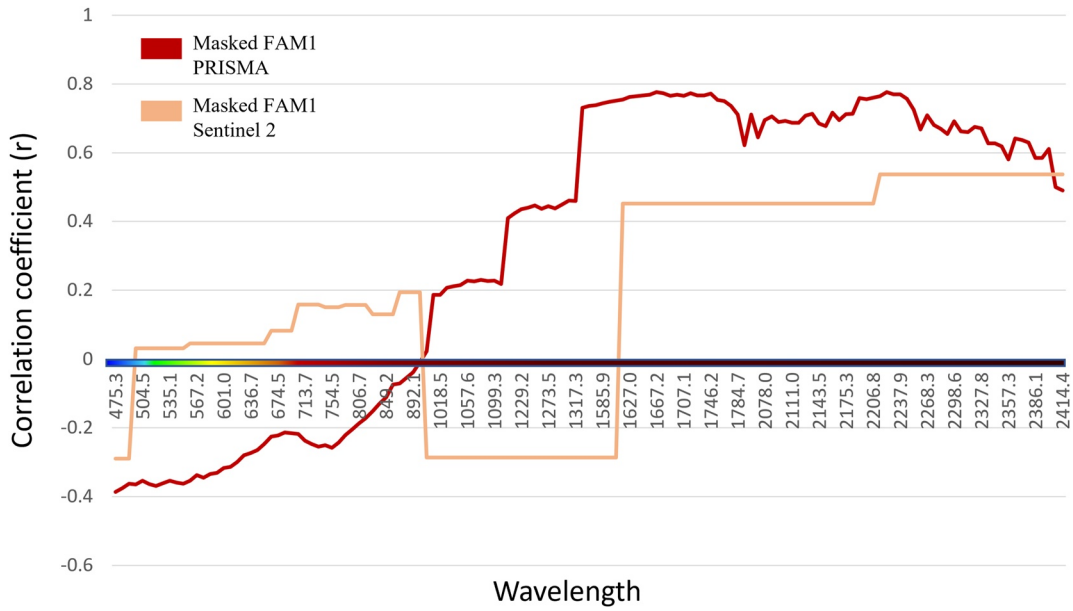

Figure 10. In red correlations of PRISMA masked-FAM1 > 0.5 and the 141 PRISMA spectral bands (wavelengths); in orange correlation of Sentinel 2-like masked-FAM1 > 0.5 and the 12 spectral bands of Sentinel 2.

Maccarese farmland was more suited to test the relevance of the SWIR region for soil texture class retrieval because of the availability of contemporary acquisitions of images from PRISMA hyperspectral and Sentinel-2 multispectral sensors. The area, being influenced by coastal sediment transport, is characterized by high percentage of sand and the LSMA provided good accuracy with hyperspectral data for 2 FAMs, one related to the medium sand class (PA = 66%) and the other to the high silt class (PA = 48.8%) while Sentinel 2 configuration, provided accurate results for two FAMs but only for high silt class (PA = 80%) and medium clay class (PA = 62.2%) (Table S2 in Supporting Information S1). These results confirm the ability of hyperspectral imaging to identify the spatial patterns of fine (silt and clay) and coarse (sand) textures since both sensors show the highest positive correlation values for the SWIR wavelengths, but PRISMA performances are higher (r = 0.7) than Sentinel 2 (r = 0.5) (Figure 9) in this spectral region (>1,300 nm). The evidence of the validity of the spectral – spatial processing path identified in the study is also revealed by the patterns identified in Maccarese with the two sensors. In Figure 9 and Figure S2 in Supporting Information S1, while PRISMA FAMs identify distributed fractional coverage behavior similar to USDA classification, in the Sentinel 2 derived FAMs of the same dates, the pattern is striped all through the area. In particular, unless the road that divide the area in two subunits and the trees in the southern apex, correctly identified by both sensors, it seems that Sentinel 2 is responding to the plowing of the soil instead the hyperspectral is accounting for the spatial pattern of soil properties. The PRISMA FAM3 has been interpreted as affected by sparse NPV presence, considering that in July the harvest phases could determine the presence of dry-dead vegetation residuals as observed in Pepe et al., 2020.

The initial hypothesis of the presented study was driven by the idea of finding direct relation between the soil texture properties in terms of sand, silt and clay abundances and the EMs spectral responses. This should have provided a bundle of EMs correlated with the kriging estimation maps. But these analyses (unpublished) didn't provide any physical, reliable results. This observation provided the chance of investigating a more powerful hypotheses related to the soil classification following a USDA meaning. In fact, the EMs in both sites provided a more evident relation with the spatial patterns of USDA maps than with the single textures' components. This path of study is more inclusive in the direction of thematic mapping, and it is also of interest for agricultural practitioners who do not need to know the grain size composition of each centimeter of field. Instead, when practicing precision farming, they would have major benefit from a thematic product informing about the main texture class of each farmland unit. The strength of the study is related to the large amount of validation data for each farmland unit supporting the accuracy of the spectral variability retrieval through the LSMA. Each fractional abundance map, classified in three intervals of values, is validated trough the confusion matrix with a high number of ground truthing samples providing robust levels of reliability.

This paper confirms that the SWIR spectral range 2,000–2,400 nm is the most relevant part of the spectrum for topsoil properties retrieval. One of the issues with hyperspectral satellite sensors is related to the fact that the quantitative predictions of soil properties were hampered by a very low SNR ratio in the SWIR region (i.e., Hyperion onboard EO1 satellite and CHRIS onboard PROBA satellite). Unfortunately, the sensor's noise generally increases when increasing the spectral resolution, thus, the advantages of detecting specific narrow bands offers the chance to consider a trade-off between a low SNR, especially in the SWIR spectral region (Lobell & Asner, 2002) and an improved revisit time, now targeted for CHIME to 10–12.5 days. Given these considerations, the improvement of the spectral characteristics of CHIME could address an optimization between the spectral ranges of interest and the satellite revisit time.

Lastly, the choice of targeting the retrieval to the widely used USDA Topsoil Texture classification for future developments of thematic maps could represent a valid contribution to enrich the Copernicus Land Monitoring Service with a collection of operational products. The topsoil texture is a geophysical variable at the interface between Land Cover and Land Use, then perfectly matching the objectives of the EAGLE (EIONET Action Group on Land monitoring in Europe) data model. Land cover and land use are often combined in practical applications (e.g., croplands) and the ambition of the EAGLE model is to build a framework for the integration of land cover and land use (LC/LU) information from various data sets. In this way, the operational services could feed strategies and directives towards more sustainable agricultural practices in support to the guidelines of good agricultural practices provided by the FAO and the objectives of the CAP.

5. Conclusions

This study explores the potential of hyperspectral data for topsoil texture classes detection with linear spectral mixture models. The work develops a mostly image-based topsoil classification model considering how costly field sampling for validation and calibration of biophysical retrieval models can be. The strategy of working with the relative proportions of coarse and fine textures to target the detection of USDA Soil Texture Classification proved to be feasible.

The two farmland units have been analyzed with hyperspectral and multispectral configurations and the second is able to provide a reduced number of validated fractional abundance intervals in both sites. The discrimination of specific spatial patterns in relation to the spectral variability across pixels was obtained thanks to the SWIR of hyperspectral CHIME-like and PRISMA configuration. The use of different hyperspectral data provided similar results in the two areas with a set of fractional abundances having the highest spatial agreement with the USDA class cover and highlighting spatial patterns unrevealed through an identical processing path with multispectral. These fractional abundances mostly overlap the USDA clay loam soil texture classes.

These results, leverage the opportunity of extending the processing chain to a larger number of case studies and to test automatic method for collecting EMs, to better understand the physical relation between the spectral reflectance captured by the hyperspectral sensor and the spatial patterns of soil texture classes.

Regarding the future of satellite hyperspectral data, sub-pixel analyses provide a fruitful environment for creating soil texture classifications, cover types and cover mixtures. Nowadays the method could be of interest to support the creation of auxiliary layers and masks to be added in the Level 2 of future CHIME data (e.g., masks of bare soils and fractional abundance of the associated spectral variability), facilitating the use of labeled techniques like machine learning and artificial intelligence algorithms to retrieve soil textures.

Data Availability Statement

The image processing is from ENVI® (version 5.6.3) software and the data set is available at: Valentini (2023). Our analyses are based on the use of different hyperspectral data and the study of the synergies among different sensors, namely hyperspectral satellite data from the PRISMA mission (ASI), multispectral satellite data from the Sentinel 2 mission (ESA) and hyperspectral airborne data from AVIRIS-NG (NASA) resampled to CHIME and Sentinel 2 spatial and spectral features. Field campaigns datasets are available for the two croplands (Valentini, 2023).

Acknowledgments
This research was funded by the CHEES Chime End to End Mission Performance Simulator ISPRA-GMV Contract No. GMVAD CHEES/ISPRA 30747/22 and the CHIME Mission Requirement Consolidation Study (RCS) (ESA Contract 4000125506/18/NL/IA) both funded by the European Space Agency (ESA). A special acknowledgment goes to the CNR–IREA group for supporting the field data collection and laboratory analyses. RC and SP acknowledge co-funding from the Italian Space Agency (ASI) within the TEHRA project (contract 2022-6-U.0). Project carried out using ORIGINAL PRISMA Products—© Italian Space Agency (ASI); the Products have been delivered under an ASI License to Use. This paper and related research have been conducted during and with the support of the Italian national inter-university PhD course in Sustainable Development and Climate change (link: www.phd-sdc.it).

References

Arrouays, D., Lagacherie, P., & Hartemink, A. E. (2017). Digital soil mapping across the globe. *Geoderma Regional*, *9*, 1–4. https://doi.org/10.1016/J.GEODRS.2017.03.002

Bachmann, M., Alonso, K., Carmona, E., Gerasch, B., Habermeyer, M., Holzwarth, S., et al. (2021). Analysis-ready data from hyperspectral sensors—The design of the EnMAP card4l-SR data product. *Remote Sensing*, *13*(22), 4536. https://doi.org/10.3390/RS13224536/S1

Ben-Dor, E., Chabrillat, S., & Demattê, J. A. M. (2018). Characterization of soil properties using reflectance spectroscopy. *Fundamentals, Sensor Systems, Spectral Libraries, and Data Mining for Vegetation*, 187–247. https://doi.org/10.1201/9781315164151-8

Ben-Dor, E., Chabrillat, S., Demattê, J. A. M., Taylor, G. R., Hill, J., Whiting, M. L., & Sommer, S. (2009). Using Imaging Spectroscopy to study soil properties. *Remote Sensing of Environment*, *113*(SUPPL. 1), S38–S55. https://doi.org/10.1016/J.RSE.2008.09.019

Blott, S. J., & Pye, K. (2012). Particle size scales and classification of sediment types based on particle size distributions: Review and recommended procedures. *Sedimentology*, *59*(7), 2071–2096. https://doi.org/10.1111/J.1365-3091.2012.01335.X

Boardman, J. W. (1995). Analysis, understanding, and visualization of hyperspectral data as convex sets in n space, (Vol. *2480*, 14–22). https://doi.org/10.1117/12.210878

Bouma, J., Pinto-Correia, T., & Systems, C. V.-S. (2021). *Assessing the role of soils when developing sustainable agricultural production systems focused on achieving the UN-SDGs and the EU green deal*. Mdpi.Com. https://doi.org/10.3390/soilsystems5030056

Candiani, G., Tagliabue, G., Panigada, C., Verrelst, J., Picchi, V., Caicedo, J. P. R., & Boschetti, M. (2022). Evaluation of hybrid models to estimate chlorophyll and nitrogen content of maize crops in the framework of the future CHIME mission. *Remote Sensing*, *14*(8), 1792. https://doi.org/10.3390/RS14081792

Casa, R., Castaldi, F., Pascucci, S., Palombo, A., & Pignatti, S. (2013). A comparison of sensor resolution and calibration strategies for soil texture estimation from hyperspectral remote sensing. *Geoderma*, *197–198*, 17–26. https://doi.org/10.1016/J.GEODERMA.2012.12.016

Casa, R., Pignatti, S., Pascucci, S., Huang, W., & Pepe, M. (2020). Effect of spatial resolution on soil properties retrieval from imaging spectroscopy: An assessment of the hyperspectral Chime mission potential. *International Geoscience and Remote Sensing Symposium (IGARSS)*, 4906–4909. https://doi.org/10.1109/IGARSS39084.2020.9323268

Castaldi, F., Palombo, A., Santini, F., Pascucci, S., Pignatti, S., & Casa, R. (2016). Evaluation of the potential of the current and forthcoming multispectral and hyperspectral imagers to estimate soil texture and organic carbon. *Remote Sensing of Environment*, *179*, 54–65. https://doi.org/10.1016/J.RSE.2016.03.025

Chabrillat, S., Ben-Dor, E., Cierniewski, J., Gomez, C., Schmid, T., & van Wesemael, B. (2019). Imaging spectroscopy for soil mapping and monitoring. *Surveys in Geophysics*, *40*(3), 361–399. https://doi.org/10.1007/S10712-019-09524-0

Cogliati, S., Sarti, F., Chiarantini, L., Cosi, M., Lorusso, R., Lopinto, E., et al. (2021). The PRISMA imaging spectroscopy mission: Overview and first performance analysis. *Remote Sensing of Environment*, *262*, 112499. https://doi.org/10.1016/J.RSE.2021.112499

Davis, R. O. E., & Bennett, H. H. (1927). *Grouping of soils on the basis of mechanical analysis*. US Department of Agriculture. Retrieved from https://scholar.google.com/scholar?hl=it&as_sdt=0%2C5&q=Davis+and+Bennett%3B1927&btnG=#d=gs_cit&t=1677492010221&u=%2Fscholar%3Fq%3Dinfo%3AReb4VhNTdPEJ%3Ascholar.google.com%2F%26output%3Dcite%26scirp%3D0%26hl%3Dit

Ding, J., & Eldridge, D. J. (2022). Drivers of soil biodiversity vary with organism type along an extensive aridity gradient. *Applied Soil Ecology*, *170*, 104271. https://doi.org/10.1016/J.APSOIL.2021.104271

Ditzler, C., Scheffe, K., & Monger, H. C. (2017). Soil Survey Manual | Natural Resources Conservation Service. Retrieved from https://www.nrcs.usda.gov/resources/guides-and-instructions/soil-survey-manual

FAO-ISRIC-ISSS. (2007). World reference base for soil resources. World Soil Resources Report 103. Rome: Food and Agriculture Organization of the United Nations (2006), pp. 132, US$22.00 (paperback). ISBN 92-5-10511-4. *Experimental Agriculture*, *3*(2), 264. https://doi.org/10.1017/S0014479706394902

Food and Agriculture Organization of the United Nations (1998). World reference base for soil resources (Vol. *88*).

Gholizadeh, A., Žižala, D., Saberioon, M., & Borůvka, L. (2018). Soil organic carbon and texture retrieving and mapping using proximal, airborne and Sentinel-2 spectral imaging. *Remote Sensing of Environment*, *218*, 89–103. https://doi.org/10.1016/J.RSE.2018.09.015

Gomez, C., Drost, A. P. A., & Roger, J. M. (2015). Analysis of the uncertainties affecting predictions of clay contents from VNIR/SWIR hyperspectral data. *Remote Sensing of Environment*, *156*, 58–70. https://doi.org/10.1016/J.RSE.2014.09.032

Green, R. O., & Thompson, D. R. (2021). NASA'S earth surface mineral dust source investigation: AN earth venture imaging spectrometer science mission. *International Geoscience and Remote Sensing Symposium (IGARSS)*, 119–122. https://doi.org/10.1109/IGARSS47720.2021.9554217

Guanter, L., Kaufmann, H., Segl, K., Foerster, S., Rogass, C., Chabrillat, S., et al. (2015). The EnMAP spaceborne imaging spectroscopy mission for Earth observation. *Remote Sensing*, *7*(7), 8830–8857. https://doi.org/10.3390/RS70708830

Guerra, C. A., Rosa, I. M. D., Valentini, E., Wolf, F., Filipponi, F., Karger, D. N., et al. (2020). Global vulnerability of soil ecosystems to erosion. *Landscape Ecology*, *35*(4), 823–842. https://doi.org/10.1007/S10980-020-00984-Z/FIGURES/5

Jabro, J. D., Evans, R. G., Kim, Y., & Iversen, W. M. (2009). Estimating in situ soil-water retention and field water capacity in two contrasting soil textures. *Irrigation Science*, *27*(3), 223–229. https://doi.org/10.1007/S00271-008-0137-9/METRICS

Krutz, D., Müller, R., Knodt, U., Günther, B., Walter, I., Sebastian, I., et al. (2019). The instrument design of the DLR Earth sensing imaging spectrometer (DESIS). *Sensors*, *19*(7), 1–16. https://doi.org/10.3390/s19071622

Lee, C. M., Cable, M. L., Hook, S. J., Green, R. O., Ustin, S. L., Mandl, D. J., & Middleton, E. M. (2015). An introduction to the NASA Hyperspectral InfraRed Imager (HyspIRI) mission and preparatory activities. *Remote Sensing of Environment*, *167*, 6–19. https://doi.org/10.1016/J.RSE.2015.06.012

Lobell, D. B., & Asner, G. P. (2002). Moisture effects on soil reflectance. *Soil Science Society of America Journal*, *66*(3), 722–727. https://doi.org/10.2136/SSSAJ2002.7220

Matsunaga, T., Iwasaki, A., Tachikawa, T., Tanii, J., Kashimura, O., Mouri, K., et al. (2022). The status and early results of hyperspectral imager suite (HISUI). In *International Geoscience and Remote Sensing Symposium (IGARSS)* (pp. 5399–5400). https://doi.org/10.1109/IGARSS46834.2022.9883526

Moeys, J. (2018). The soil texture wizard: R functions for plotting, classifying, transforming and exploring soil texture data.

Mohamed, E. S., Saleh, A. M., Belal, A. B., & Gad, A. A. (2018). Application of near-infrared reflectance for quantitative assessment of soil properties. *The Egyptian Journal of Remote Sensing and Space Science*, *21*(1), 1–14. https://doi.org/10.1016/J.EJRS.2017.02.001

Mzid, N., Castaldi, F., Tolomio, M., Pascucci, S., Casa, R., & Pignatti, S. (2022). Evaluation of agricultural bare soil properties retrieval from Landsat 8, Sentinel-2 and PRISMA satellite data. *Remote Sensing*, *14*(3), 714. https://doi.org/10.3390/RS14030714

Nieke, J., & Rast, M. (2018). Towards the copernicus hyperspectral imaging mission for the environment (CHIME). In *International Geoscience and Remote Sensing Symposium (IGARSS)* (pp. 157–159). https://doi.org/10.1109/IGARSS.2018.8518384

Pebesma, E. J. (2004). Multivariable geostatistics in S: The gstat package. *Computers and Geosciences*, *30*(7), 683–691. https://doi.org/10.1016/J.CAGEO.2004.03.012

Pepe, M., Pompilio, L., Gioli, B., Busetto, L., & Boschetti, M. (2020). Detection and classification of non-photosynthetic vegetation from PRISMA hyperspectral data in croplands. *Remote Sensing*, *12*(23), 1–12. https://doi.org/10.3390/rs12233903

Phogat, V. K., Tomar, V., & Dahiya, R. (2015). Soil physical properties. *Soil science: An introduction*, (pp. 135–171). Retrieved from https://www.researchgate.net/publication/297737054

Plaza, A., Martínez, P., Pérez, R., & Plaza, J. (2002). Spatial/spectral endmember extraction by multidimensional morphological operations. *IEEE Transactions on Geoscience and Remote Sensing*, *40*(9), 2025–2041. https://doi.org/10.1109/TGRS.2002.802494

Rast, M., Ananasso, C., Bach, H., Ben-Dor, E., Chabrillat, S., Colombo, R., et al. (2019). ESA UNCLASSIFIED-for Official use copernicus hyperspectral imaging mission for the environment-mission requirements document. In *Mission requirements Document (MRD); No. ESA-EOPSM-CHIM-MRD-3216*. European Space Agency (ESA). Retrieved from www.esa.int

Rawls, W. J., Pachepsky, Y. A., Ritchie, J. C., Sobecki, T. M., & Bloodworth, H. (2003). Effect of soil organic carbon on soil water retention. *Geoderma*, *116*(1–2), 61–76. https://doi.org/10.1016/S0016-7061(03)00094-6

Safanelli, J. L., Chabrillat, S., Ben-Dor, E., & Demattê, J. A. M. (2020). Multispectral models from bare soil composites for mapping topsoil properties over Europe. *Remote Sensing*, *12*(9), 1369. https://doi.org/10.3390/RS12091369

Seaton, F. M., George, P. B. L., Lebron, I., Jones, D. L., Creer, S., & Robinson, D. A. (2020). Soil textural heterogeneity impacts bacterial but not fungal diversity. *Soil Biology and Biochemistry*, *144*, 107766. https://doi.org/10.1016/J.SOILBIO.2020.107766

Silvestro, P. C., Casa, R., Hanuš, J., Koetz, B., Rascher, U., Schuettemeyer, D., et al. (2021). Synergistic use of multispectral data and crop growth modelling for spatial and temporal evapotranspiration estimations. *Remote Sensing*, *13*(11), 2138. https://doi.org/10.3390/RS13112138

Sousa, D., Brodrick, P., Cawse-Nicholson, K., Fisher, J. B., Pavlick, R., Small, C., & Thompson, D. R. (2022). The spectral mixture residual: A source of low-variance information to enhance the explainability and accuracy of surface Biology and Geology retrievals. *Journal of Geophysical Research: Biogeosciences*, *127*(2), e2021JG006672. https://doi.org/10.1029/2021JG006672

Sousa, D., & Small, C. (2018). Multisensor analysis of spectral dimensionality and soil diversity in the Great Central Valley of California. *Sensors*, *18*(2), 583. https://doi.org/10.3390/S18020583

Taramelli, A., Lissoni, M., Piedelobo, L., Schiavon, E., Valentini, E., Xuan, A. N., & González-Aguilera, D. (2019). Monitoring green infrastructure for natural water retention using copernicus global land products. *Remote Sensing*, *11*(13), 1583. https://doi.org/10.3390/RS11131583

Taramelli, A., Tornato, A., Magliozzi, M. L., Mariani, S., Valentini, E., Zavagli, M., et al. (2020). An interaction methodology to collect and assess user-driven requirements to define potential opportunities of future hyperspectral imaging Sentinel mission. *Remote Sensing*, *12*(8), 1286. https://doi.org/10.3390/rs12081286

Vaezi, A. R., Hasanzadeh, H., & Cerdà, A. (2016). Developing an erodibility triangle for soil textures in semi-arid regions, NW Iran. *CATENA*, *142*, 221–232. https://doi.org/10.1016/J.CATENA.2016.03.015

Valentini, E. (2023). Hyperspectral mixture models in the CHIME mission implementation for topsoil texture retrieval [Dataset]. Zenodo. https://doi.org/10.5281/zenodo.7805448

Valentini, E., Taramelli, A., Cappucci, S., Filipponi, F., & Xuan, A. N. (2020). Exploring the dunes: The correlations between vegetation cover pattern and morphology for sediment retention assessment using airborne multisensor acquisition. *Remote Sensing*, *12*(8), 1229. https://doi.org/10.3390/RS12081229

Veganzones, M. A., & Graña, M. (2008). Endmember extraction methods: A short review. *Lecture Notes in Computer Science*, *5179*, 400–407. *LNAI*(PART 3). https://doi.org/10.1007/978-3-540-85567-5_50/COVER

Viscarra Rossel, R. A., Adamchuk, V. I., Sudduth, K. A., McKenzie, N. J., & Lobsey, C. (2011). Proximal soil sensing: An effective approach for soil measurements in space and time. *Advances in Agronomy*, *113*, 243–291. https://doi.org/10.1016/B978-0-12-386473-4.00005-1

Viscarra Rossel, R. A., Behrens, T., Ben-Dor, E., Brown, D. J., Demattê, J. A. M., Shepherd, K. D., et al. (2016). A global spectral library to characterize the world's soil. *Earth-Science Reviews*, *155*, 198–230. https://doi.org/10.1016/J.EARSCIREV.2016.01.012

Viscarra Rossel, R. A., Walvoort, D. J. J., McBratney, A. B., Janik, L. J., & Skjemstad, J. O. (2006). Visible, near infrared, mid infrared or combined diffuse reflectance spectroscopy for simultaneous assessment of various soil properties. *Geoderma*, *131*(1–2), 59–75. https://doi.org/10.1016/J.GEODERMA.2005.03.007

Xie, Q., Dash, J., Huang, W., Peng, D., Qin, Q., Mortimer, H., et al. (2018). Vegetation indices combining the red and red-edge spectral information for leaf area index retrieval. *Ieee Journal of Selected Topics in Applied Earth Observations and Remote Sensing*, *11*(5), 1482–1492. https://doi.org/10.1109/JSTARS.2018.2813281